Available online at www.sciencedirect.com
SCIENCE DIRECT®
Geochimica et Cosmochimica Acta 70 (2006) 2073–2092
Geochimica
www.elsevier.com/locate/gca

Geochemistry of low-molecular weight hydrocarbons in hydrothermal fluids from Middle Valley, northern Juan de Fuca Ridge

Anna M. Cruse *, Jeffrey S. Seewald

Department of Marine Chemistry and Geochemistry, Woods Hole Oceanographic Institution, Woods Hole, MA 02543, USA

Received 31 March 2005; accepted in revised form 18 January 2006

Abstract

Hydrothermal vent fluids from Middle Valley, a sediment-covered vent field located on the northern Juan de Fuca Ridge, were sampled in July, 2000. Eight different vents with exit temperatures of 186–281 °C were sampled from two areas of venting: the Dead Dog and ODP Mound fields. Fluids from the Dead Dog field are characterized by higher concentrations of ΣNH_3 and organic compounds (C_1–C_4 alkanes, ethene, propene, benzene and toluene) compared with fluids from the ODP Mound field. The ODP Mound fluids, however, are characterized by higher $C_1/(C_2 + C_3)$ and benzene:toluene ratios than those from the Dead Dog field. The aqueous organic compounds in these fluids have been derived from both bacterial processes (methanogenesis in low temperature regions during recharge) as well as from thermogenic processes in higher temperature portions of the subsurface reaction zone. As the sediments undergo hydrothermal alteration, carbon dioxide and hydrocarbons are released to solution as organic matter degrades via a stepwise oxidation process. Compositional and isotopic differences in the aqueous hydrocarbons indicate that maximum subsurface temperatures at the ODP Mound are greater than those at the Dead Dog field. Maximum subsurface temperatures were calculated assuming that thermodynamic equilibrium is attained between alkenes and alkanes, benzene and toluene, and carbon dioxide and methane. The calculated temperatures for alkene–alkane equilibrium are consistent with differences in the dissolved Cl concentrations in fluids from the two fields, and confirm that subsurface temperatures at the ODP Mound are hotter than those at the Dead Dog field. Temperatures calculated assuming benzene–toluene equilibrium and carbon dioxide–methane equilibrium are similar to observed exit temperatures, and do not record the hottest subsurface conditions. The difference in subsurface temperatures estimated using organic geochemical thermometers reflects subsurface cooling processes via mixing of a hot, low salinity vapor with a cooler, seawater salinity fluid. Because of the disparate temperature dependence of alkene–alkane and benzene–toluene equilibria, the mixed fluid records both the high and low temperature equilibrium conditions. These calculations indicate that vapor-rich fluids are presently being formed in the crust beneath the ODP Mound, yet do not reach the surface due to mixing with the lower temperature fluids.

1. Introduction

The Middle Valley hydrothermal system is located at the northern end of the Juan de Fuca Ridge, where up to 1.5 km of hemipelagic and turbiditic sediments overlie the ridge axis (Davis et al., 1992). In these systems, hydrothermal venting occurs in two main regions located approximately 4 km apart: the Dead Dog and ODP Mound vent fields (Davis and Villinger, 1992; Fig. 1A). Hydrothermal fluids interact with both oceanic basalt as well as overlying sediments. Thermal alteration of sedimentary organic matter results in the release to solution of myriad organic alteration products that can be key to many processes occurring at mid-ocean ridges, such as the transport of metals in solution and the formation of massive sulfide deposits (Disnar and Sureau, 1990; Cruse and Seewald, 2001, and references therein; Martens, 1990; Simoneit, 1994). These compounds also represent carbon and energy sources for the large and diverse

* Corresponding author. Present address: Oklahoma State University, School of Geology, 105 Noble Research Center, Stillwater, OK 74078-3031, USA. Fax: +1 405 744 7841.
E-mail address: anna.cruse@okstate.edu (A.M. Cruse).

0016-7037/$ - see front matter © 2006 Elsevier Inc. All rights reserved.
doi:10.1016/j.gca.2006.01.015

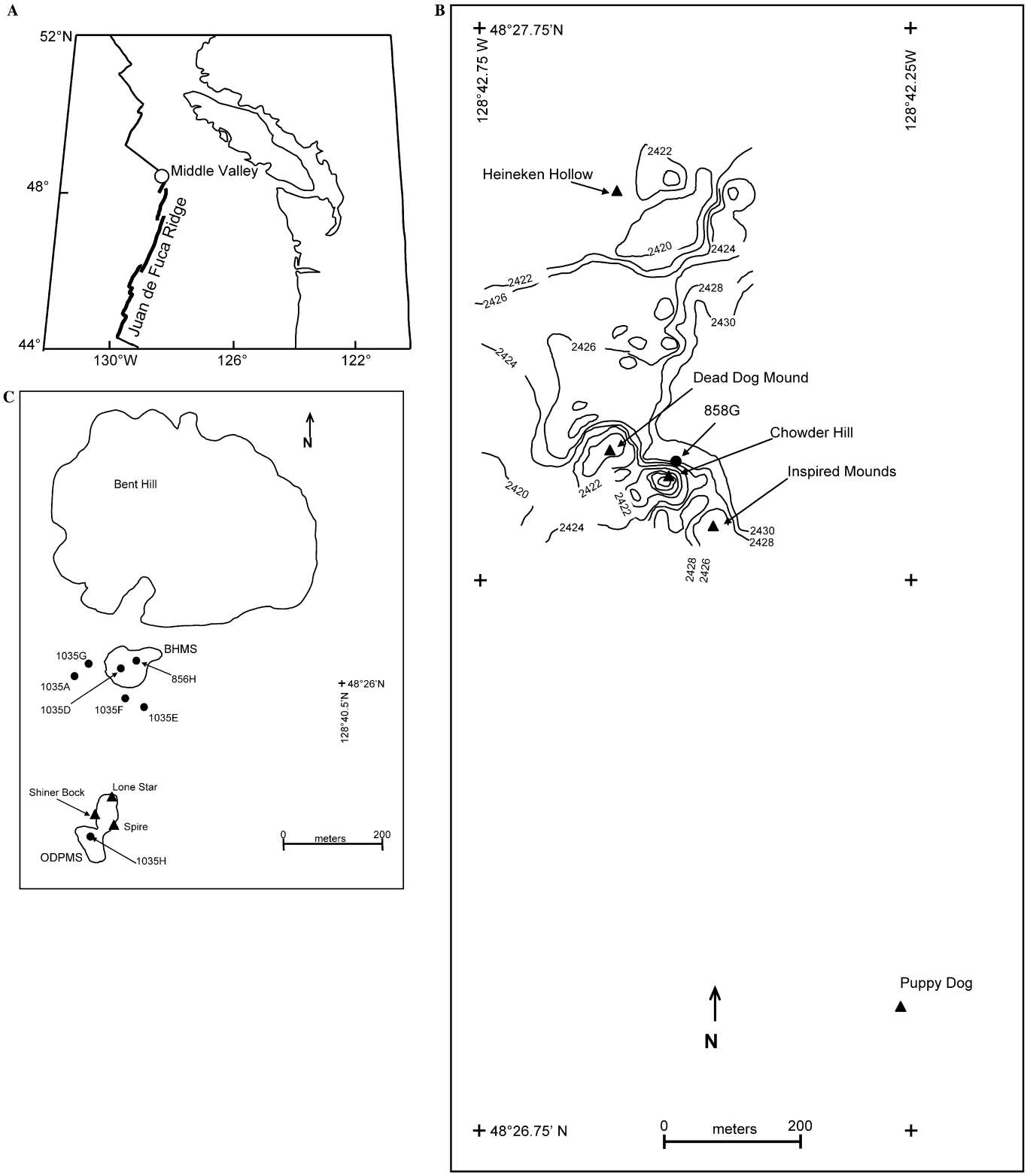

Fig. 1. Location maps of (A) Middle Valley field on the Juan de Fuca Ridge, (B) Dead Dog and (C) ODP Mound vent fields. Sampled vents are indicated with triangles, and ODP drillholes are indicated with circles. Contours on (B) are drawn at 2 m intervals. Figures are modified from Zierenberg and Miller (2000).

biological communities that inhabit hydrothermal vent environments (Hessler and Kaharl, 1995).

Organic compounds can also serve as geochemical indicators of the conditions under which fluid–rock interactions occur in subsurface reaction zones, where direct measurements cannot yet be made. In conventional models of organic matter alteration, the amounts and isotopic compositions of alteration products are controlled by

kinetic factors (Tissot and Welte, 1984; Hunt, 1996). Recent theoretical and laboratory work, however, suggests that metastable thermodynamic equilibrium among organic compounds, inorganic minerals and water may regulate the abundances of compounds such as carbon dioxide, hydrocarbons and organic acids (Shock, 1988, 1989, 1992; Helgeson, 1991; Helgeson et al., 1993; Seewald, 1994, 1997, 2001a,b; McCollom et al., 2001). The concentrations and isotopic compositions of organic compounds in hydrothermal vent fluids can be analyzed within the framework of such models to constrain subsurface conditions and to better understand crustal alteration processes.

In contrast to numerous studies reporting the abundance of inorganic aqueous species in ridge-crest hydrothermal fluids, quantitative data for the concentration and isotopic composition of low molecular weight hydrocarbons and CO_2 in vent fluids from sedimented systems are more limited. Here we report the chemical and isotopic compositions of aqueous carbon species in vent fluids collected from Middle Valley in July, 2000. These data are used to determine sources of carbon and reactions that control the distribution and abundance of organic compounds in sediment-covered hydrothermal systems.

2. Experimental

2.1. Geologic setting

Middle Valley is an axial rift valley located on the northern edge of the Juan de Fuca Ridge (Fig. 1A). At this location, the ridge is spreading at an intermediate rate of 30 mm/yr (half-rate; Goodfellow and Blaise, 1988). Terrestrial and hemipelagic sediments derived from the continental shelf filled Middle Valley during Pleistocene sea-level lowstands. The sediment cover ranges in thickness from a few hundred meters in the south to 1.5 km in the north (Goodfellow and Blaise, 1988). Sedimentation was contemporaneous with active extension and volcanism, creating an uppermost basement that consists of a basaltic-sill/sediment complex (Davis and Villinger, 1992). Past hydrothermal activity has formed two seafloor massive sulfide deposits: the Bent Hill massive sulfide deposit (BHMS), which is estimated to contain over 8 million tons of ore, and the smaller, younger ODP Mound massive sulfide deposit (Zierenberg et al., 1998).

Vent sites at the Dead Dog field consist of mounds, ranging from 5 to 15 m high and 10 to 30 m in diameter. A single large chimney 1–5 m high is usually located on the top of each mound, while smaller (<2 m) spires can be located on the sides. In many instances, diffuse flow (shimmering water) can be seen emanating from the sulfide rubble and sediments that make up the mounds, or from the base of the chimney itself. The chimneys are dominantly composed of anhydrite, often with an inner lining of magnesium smectite coating the active flow conduits, and contain minor disseminated pyrrhotite, sphalerite, isocubanite, chalcopyrite, and galena (Ames et al., 1993). Fluids were collected at four sites: Heineken Hollow, Inspired Mounds, Chowder Hill, and Puppy Dog (Fig. 1B).

Prior to drilling during ODP Leg 169 in 1996, known venting at the ODP Mound area was limited to the Lone Star vent on the northern flank of the ODP Mound massive sulfide (Fig. 1C; Butterfield et al., 1994a; Zierenberg and Miller, 2000). During a camera survey to spud Hole 1035H during Leg 169, a second area of hydrothermal venting was tentatively identified approximately 30 m to the north of Hole 1035H (Fig. 1C; Zierenberg and Miller, 2000). A small area of hydrothermal venting was later confirmed during an *Alvin* dive in 1998 and hydrothermal fluids were sampled from a 1.5 m high anhydrite chimney named Shiner Bock vent (Fig. 1C; Zierenberg and Miller, 2000). Finally, hydrothermal fluid was also observed to be venting from drillholes 1035F and 1035H during Leg 169 operations (Shipboard Scientific Party, 1998a). It is hypothesized that a silicified layer discovered at ~150 mbsf acted as a hydrologic seal, and that puncturing of this layer during drilling allowed flow of previously confined fluids (Shipboard Scientific Party, 1998a; Zierenberg and Miller, 2000; Gieskes et al., 2002).

Hydrothermal fluids were discharging from drillholes 1035F, 1035H and 1035G (Fig. 1C) when visited during this study in July, 2000. Site 1035H is unique in that a 10 m tall anhydrite structure had formed over the drillhole since 1998 when a similar structure collapsed during sampling operations with *Alvin* (Zierenberg, private communication). Active venting of hydrothermal fluids was also observed in 2000 from several 0.5 to 1 m high chimneys and spires that cover the eastern area of the ODP Mound. Hydrothermal activity was not observed at this location in 1998 (Zierenberg, private communication) and therefore represents a new area of venting at the ODP Mound field that was less than two years old at the time of sampling. Fluids were sampled from Shiner Bock vent, drillhole 1035H, and from a small vent (henceforth referred to as Spire vent) in the area of new venting (Fig. 1C). Fluids from drillhole 1035F, located near the Bent Hill massive sulfide deposit were also sampled.

The discharge of hydrothermal fluids in both study areas is hypothesized to be controlled by an indurated silicified layer. The layer is located at 30 m below the seafloor (mbsf) at the Dead Dog field, and approximately 150 mbsf at the ODP Mound field (Shipboard Scientific Party, 1992, 1998a,b; Stein et al., 1998; Stein and Fisher, 2001). Recharge of vent fluids is thought to occur along the normal faults and linear unsedimented basement ridges that border Middle Valley (Stein and Fisher, 2001), rather than as diffusive flow through the sediments (Rabinowicz et al., 1998). The Dead Dog field is located over a buried basement edifice at 258 mbsf (Shipboard Scientific Party, 1992) that focuses fluid flow from the deep basement (Davis and Fisher, 1994; Golden et al., 2003). Individual vents within the Dead Dog field likely reflect localized pathways of higher permeability through the silicified layer. A region

of overpressured, high permeability basement was also apparently intersected by drillholes 1035F, 1035H, and 1035G, which provide anthropogenic conduits through the silicified layer (Shipboard Scientific Party, 1998a). Similar to the Dead Dog field, the locations of the active vents and spires that now cover the ODP Mound field likely reflect localized channels of high permeability through the 400 m of sediment overlying the basaltic basement. The initiation of widespread venting in the area of Spire vent following the drilling of hole 1035H suggests that penetration of the impermeable seal has allowed hydrothermal fluids to access preexisting conduits in the sulfide mound.

2.2. Sample collection and analysis

Vent fluid samples were collected using isobaric gas-tight fluid samplers (Seewald et al., 2002) deployed from the submersible *Alvin*. These samplers prevent degassing during ascent to the surface and shipboard processing by maintaining the fluid at seafloor pressures while subsamples are withdrawn through a micrometering valve. Two gas-tight samples were collected at each vent. Additional samples were taken from some vents using non-gas-tight titanium "major" samplers (Edmond et al., 1992; Von Damm et al., 1985). Fluids from the "major" samplers were utilized only for analysis of the non-volatile species ΣNH_3, Cl, and Mg. Reported temperatures were measured using the *Alvin* high temperature probe and are corrected by 2 °C to take into account the cold-junction temperature.

Once on board the ship, fluids were processed such that concentrations of volatile, semi-volatile and non-volatile organic and inorganic aqueous species could be measured in each gas-tight sample. Subsamples for H_2 and CH_4 analysis were withdrawn into glass gas-tight syringes and analyzed in the shipboard laboratory. Fluid aliquots for the determination of CO_2 were stored in evacuated 30 mL culture tubes that had been previously combusted at 400 °C and sealed with butyl rubber stoppers. A subset of the culture tubes was also pre-spiked with $HgCl_2$ to prevent microbial activity. No difference in measured CO_2 concentrations was detected between Hg-treated and -untreated samples. Samples for determination of the aqueous concentrations of low-molecular weight volatile organic compounds (C_2–C_4 alkenes and alkanes, benzene and toluene) and the isotopic composition of CO_2, C_1–C_4 alkanes, benzene and toluene were withdrawn into evacuated 6 or 9 mm ID Pyrex® glass tubes fitted with gas-tight valves. After filling, the tubes were stored at 5 °C with their valves submerged in water until analyzed at WHOI. Samples for the determination of Cl, Mg, and ΣNH_3 were stored in acid-cleaned polyethylene bottles at 5 °C. The concentrations of species measured at sea are reported in units of μmol/L or mmol/L fluid, while data for species measured on shore are reported in units of μmol/kg fluid (Tables 1 and 2). For fluids of seawater salinity and less, conversion between these two units influences the reported concentrations by <2%.

Aqueous H_2 and CH_4 concentrations were measured by gas chromatography (thermal conductivity detection) following a headspace extraction. The analytical uncertainty for these analyses (1σ) was <4%. Concentrations of Cl, Ca, Na, K, and Mg were measured using ion chromatography with estimated uncertainties of ±2%. ΣNH_3 ($NH_{3(aq)} + NH_4^+$) concentrations were determined spectrophotometrically by flow injection analysis using the Berthelot reaction (Koroleff, 1976), with estimated uncertainties of ±5%.

CO_2 concentrations were determined by adding 5 mL of 25% phosphoric acid to the fluid in the culture tube and sparging the evolved gas into a purge and trap device interfaced directly to a gas chromatograph with a Porapak-Q packed column and serially connected thermal conductivity and flame ionization detectors. The C_2–C_4 alkanes, benzene and toluene were analyzed in a similar manner on a separate fluid aliquot without the addition of phosphoric acid. Selected samples were analyzed using a purge-and-trap device interfaced to a capillary GC system to achieve lower detection limits for quantification of low-level ethene, propene and toluene concentrations. Analytical uncertainties ranged from ±5% for ethane and propane; ±10% for CO_2, ethene, propene, butane, benzene and toluene; and ±15% for *iso*-butane.

Because fluid samplers have a finite dead volume that is filled with bottom seawater prior to deployment, and seawater entrainment occurs to varying degrees during sampling, collected fluid that is collected represents a mixture between seawater and hydrothermal vent fluid. Laboratory experiments have demonstrated near quantitative removal of Mg from seawater during hydrothermal seawater–basalt interaction at temperatures, pressures and water–rock ratios that exist in ridge-crest hydrothermal systems (Bischoff and Dickson, 1975; Mottl and Holland, 1978; Seyfried and Bischoff, 1981). Therefore, the composition of endmember hydrothermal vent fluids is calculated by extrapolating the concentrations of individual species to a zero Mg concentration using linear least squares regression of vent fluid and seawater compositions (Figs. 2 and 3).

The stable carbon isotopic compositions of CO_2, C_1–C_4 alkanes, benzene and toluene were quantified using GC-isotope ratio monitoring mass spectrometry (GC-IRMS). Complete details of the analytical methods can be found in Cruse (2002). The stable carbon isotopic composition of the gases is reported using standard delta notation, where $\delta^{13}C$ is defined by the following expression:

$$\delta^{13}C\ (‰) = \left[\frac{R_S - R_{VPDB}}{R_{VPDB}}\right] \times 1000, \quad (1)$$

where R_S is the $^{13}C/^{12}C$ ratio of the sample and R_{PDB} is the $^{13}C/^{12}C$ ratio of the Vienna PDB (V_{PDB}) standard (R_{VPDB}; $^{13}C/^{12}C = 0.011180$; Zhang and Wen-Jun, 1990).

Table 1
Concentrations of inorganic aqueous species in vent fluids from Dead Dog and ODP Mound Fields, Middle Valley, Northern Juan de Fuca Ridge

Vent	Sample	Exit *T* (°C)	Mg (mmol/kg)	Cl (mmol/kg)	NH_4 (μmol/kg)	H_2 (mmol/L)	CO_2 (mmol/kg)
Dead Dog Field							
H'ken Hollow	BGT-3597-1		51.0	544	64	0.03	2.7
	BGT-3597-2		2.37	589	2792	1.5	7.0
	M-3596-12C		3.13	581	2855		
	M-3596-1C		2.25	576	2996		
	M-3597-12		45.9	557	282		
	M3597-15		27.9	554	1350		
	Endmember	67–187	0	583	3180	1.9	8.2
Chowder Hill	BGT-3596-3		1.90	572	3045	2.5	7.5
	BGT-3596-4		1.12	576	3103	2.6	9.0
	Endmember	281		575	3164	2.6	8.4
Insp. Mounds	BGT-3597-3		34.4	551	993	0.8	5.7
	BGT-3597-4		41.0	542	524	0.5	4.2
	M-3597-6C		30.3	541	1251		
	M-3597-11C		43.0	557	551		
	Endmember	255–261	0	546	2866	2.3	12
Puppy Dog	BGT-3599-3		6.16	582	2646	1.8	7.7
	BGT-3599-4		44.6	544	351	0.3	3.4
	Endmember	202	0	586	2986	2.0	8.4
ODP Mound Field							
1035F	BGT-3598-3		43.2	527	232	0.39	3.4
	M-3598-6C		46.7	542	160		
	M-3598-11C		46.7	528	121		
	Endmember	40	0	448	1263	2.1	8.2
Shiner Bock	BGT-3595-1		1.61	435	2262	8.0	11
	BGT-3595-2		3.40	439	2099	7.6	11
	M-3595-11C		5.99	444	2130		
	M-3595-6C		12.7	467	1800		
	M-3595-1C		28.7	495	1070		
	M-3595-12		3.10	443	2240		
	Endmember	272	0	434	2340	8.2	12
Spire	BGT-3595-3		1.64	434	2107	2.1	13
	BGT-3595-4		22.5	479	1264	1.2	8.5
	M-3595-15		4.12	442	2215		
	Endmember	263	0	432	2270	2.2	13
1035H	BGT-3599-1		17.0	479	1446	4.2	7.9
	BGT-3599-2		20.9	481	1262	3.7	7.6
	M-3599-12		29.3	508	938		
	M-3599-15		30.3	506	855		
	Endmember	267	0	449	2096	6.1	11
BSW[a]	M-3598-6C	2.1	53.0	543	0.8	0	2.3

Note. Samples that begin with "M" were taken in non-gas tight samplers, and were not analyzed for the volatile species H_2 and CO_2.
[a] Bottom seawater.

The GC-IRMS precision was 0.8‰ for CO_2 and CH_4 and 0.5‰ for the C_2–C_7 hydrocarbons. Measured isotopic values of the C_1–C_7 hydrocarbons reflect their isotopic composition in endmember hydrothermal fluids because negligible concentrations of these species exist in ambient seawater. Because ambient seawater contains 2.3 mmol/kg fluid ΣCO_2, the isotopic composition of CO_2 in endmember fluids must be calculated using the isotopic mass balance:

$$\delta^{13}CO_{2,END} = [\delta^{13}CO_{2,MEAS}C_{MEAS} - (\delta^{13}CO_{2,sw}C_{sw}(1-f))] / [C_{END}(f)], \quad (2)$$

where C is the measured concentration of CO_2, f is the fraction of hydrothermal fluid in the sample (calculated from the measured Mg concentration), and the subscripts END, MEAS and SW refer to the endmember, measured, and seawater components, respectively. For each vent, at least one fluid aliquot was analyzed from each of the two gas-tight samplers when possible. All analyses were

Table 2
Concentrations of organic aqueous species in vent fluids from Dead Dog and ODP Mound fields, Middle Valley, northern Juan de Fuca Ridge

Vent	Sample (unit)[a]	CH_4 (m)	C_2H_4 (n)	C_2H_6 (μ)	C_3H_6 (n)	C_3H_8 (μ)	i-C_4H_{10} (μ)	n-C_4H_{10} (μ)	Benzene (μ)	Toluene (μ)	C_1/C_2+C_3
Dead Dog Field											
H'ken Hollow	BGT-3597-1	0.45	—	4.74	1.6	1.21	0.12	0.1	0.5	0.08	
	BGT-3597-2	17.7	3.9	186	—	47.7	4.9	5.3	22	4.7	
	Endmember	22.6	4.0	236	41	60.7	6.2	6.8	28	6.0	76.1
Chowder Hill	BGT-3596-3	19.2	6.0	219	4.7	53.2	5.8	6.0	24	4.6	
	BGT-3596-4	20.3	2.9	231	2.4	56.8	6.1	6.2	22	5.0	
	Endmember	20.3	4.6	232	3.7	56.6	6.2	6.2	23	4.9	70.5
Insp. Mounds	BGT-3597-3	7.58	4.8	219	4.7	53.2	2.1	6.0	24	4.6	
	BGT-3597-4	4.88	4.3	231	2.4	56.8	1.4	6.2	22	5.0	
	Endmember	21.6	14	232	16	57.5	5.9	6.1	24	4.5	74.4
Puppy Dog	BGT-3599-3	16.4	3.4	175	—	44.3	4.4	5.2	19	3.8	
	BGT-3599-4	2.88	—	31.6	—	7.77	0.75	0.83	3.1	0.56	
	Endmember	18.5	3.8	198	—	50.1	5.0	5.9	22	4.3	74.6
ODP Mound Field											
1035F	BGT-3598-3	0.56	5.6	2.07	2.2	0.48	—	—	0.19	0.09	
	Endmember	2.99	30	11.1	12	2.58	—	—	0.99	0.09	219
Shiner Bock	BGT-3595-1	6.92	8.4	23.2	4.0	4.47	0.35	0.98	2.6	0.19	
	BGT-3595-2	6.56	7.5	23.1	3.0	4.36	0.33	0.98	2.5	0.20	
	Endmember	7.07	8.4	24.3	3.7	4.63	0.36	1.0	2.6	0.20	245
Spire	BGT-3595-3	6.52	19	23.4	5.7	4.26	0.31	0.80	2.2	0.15	
	BGT-3595-4	3.84	13	14.3	3.9	2.74	0.23	0.59	1.5	0.12	
	Endmember	6.71	20	24.3	6.1	4.48	0.34	0.87	2.3	0.17	233
1035H	BGT-3599-1	3.98	9.4	15.6	3.5	3.09	0.24	0.71	1.5	0.12	
	BGT-3599-2	3.54	—	14.3	—	2.72	0.20	0.65	1.3	—	
	Endmember	5.85	14	23.2	5.2	4.52	0.34	1.1	2.1	0.18	211
BSW[b]		0	0	0	0	0	0	0	0	0	

[a] m: mmol/L; n: nmol/kg; μ: μmol/kg.
[b] Bottom seawater.

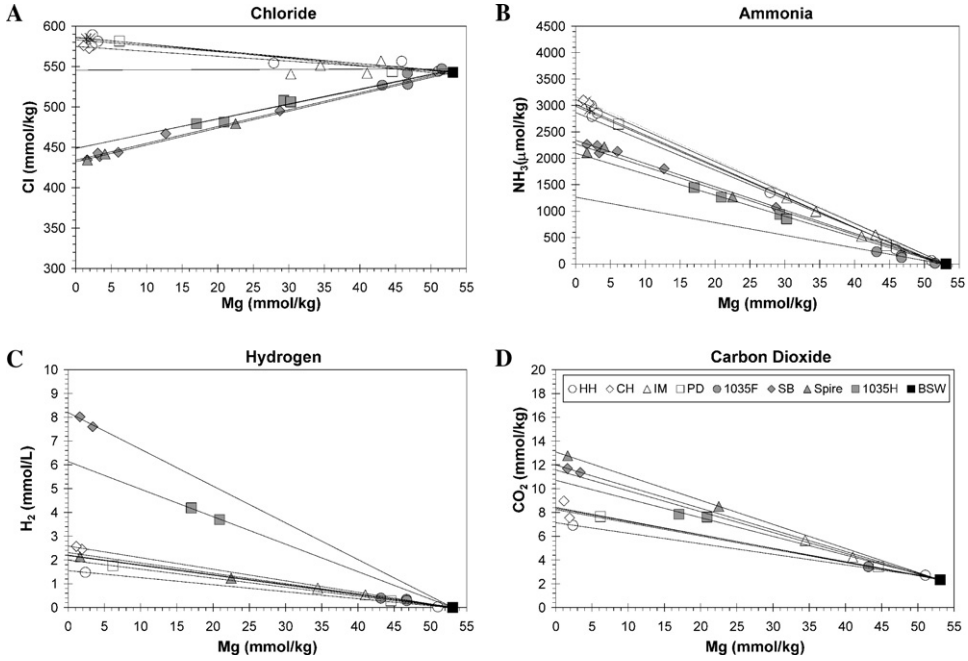

Fig. 2. Graphs of individual chemical species versus Mg in sampled vent fluids. (A) Chloride, (B) ammonia, (C) hydrogen, and (D) carbon dioxide. HH: Heineken Hollow; CH: Chowder Hill; IM: Inspired Mounds; PD: Puppy Dog; SB: Shiner Bock; BSW: Bottom seawater.

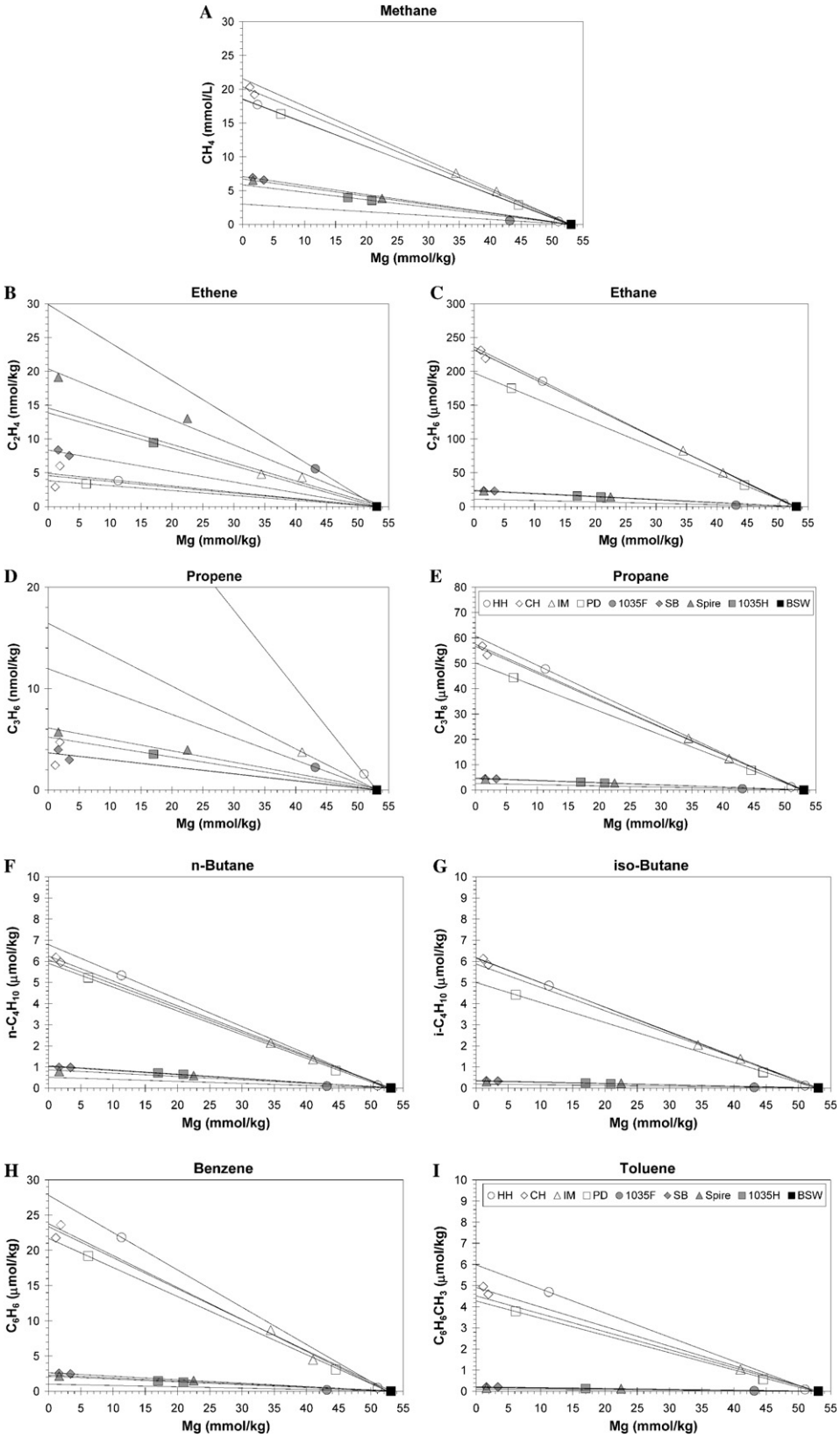

Fig. 3. Graphs of individual organic chemical species versus Mg in sampled vent fluids. (A) Methane, (B) ethene, (C) ethane, (D) propene, (E) propane, (F) *n*-butane, (G) *iso*-butane, (H) benzene, and (I) toluene. HH: Heineken Hollow; CH: Chowder Hill; IM: Inspired Mounds; PD: Puppy Dog; SB: Shiner Bock; BSW: Bottom seawater.

Table 3
Average stable carbon isotopic compositions for aqueous low-molecular weight organic compounds in vent fluids from Main Endeavour Field, northern Juan de Fuca Ridge

Vent	CO_2[a]		CH_4		C_2H_6		C_3H_8		i-C_4H_{10}		n-C_4H_{10}		Benzene		Toluene	
	$\delta^{13}C$ (‰)	1σ (n)	$\delta^{13}C$ (‰)	1σ (n)	$\delta^{13}C$ (‰)	1σ (n)	$\delta^{13}C$ (‰)	1σ (n)	$\delta^{13}C$ (‰)	1σ (n)	$\delta^{13}C$ (‰)	1σ (n)	$\delta^{13}C$ (‰)	1σ (n)	$\delta^{13}C$ (‰)	1σ (n)
Dead Dog																
Heineken Hollow	−27.8	0.2 (2)	−53.3	0.0 (2)	−20.9	0.7 (2)	−20.5	0.4 (2)	−23.6	1.8 (2)	−18.7	0.8 (2)	−23.2	0.3 (2)	−21.2	0.6 (2)
Chowder Hill	−23.8	0.5 (5)	−54.3	0.3 (5)	−21.0	0.4 (3)	−20.3	0.2 (4)	−22.8	1.1 (5)	−19.0	0.1 (5)	−23.2	0.0 (4)	−21.3	0.8 (5)
Inspired Mounds	−20.7	1.9 (9)	−55.5	1.3 (11)	−21.2	0.3 (3)	−20.3	0.3 (3)	−21.3	0.5 (4)	−18.3	0.4 (4)	−23.0	0.4 (3)	−20.2	0.1 (3)
Puppy Dog	−26.4	0.6 (6)	−54.0	0.0 (2)	−20.8	0.2 (3)	−21.0	1.3 (3)	−21.8	0.3 (2)	−19.0	0.3 (2)	−22.5	1.1 (3)	−22.3	2.4 (3)
ODP Mound																
1035F	−24.8	0.3 (5)	−53.0	0.5 (6)	−22.0	0.4 (3)	−22.3	1.0 (3)	—	—	−22.2	— (1)	−22.5	0.8 (3)	−24.4	— (1)
Shiner Bock	−34.6	0.7 (6)	−50.8	0.8 (8)	−20.6	0.4 (4)	−20.1	0.3 (4)	−22.2	0.6 (4)	−21.7	0.4 (4)	−21.5	0.3 (4)	−22.2	0.6 (4)
Spire	−33.9	0.9 (3)	−51.6	0.6 (7)	−21.8	0.3 (3)	−21.5	0.6 (3)	−25.3	— (1)	−22.1	0.5 (3)	−22.1	0.5 (3)	−23.3	— (1)
1035H	−33.4	0.6 (12)	−51.2	0.9 (9)	−22.7	1.4 (6)	−21.2	1.2 (6)	−23.5	1.2 (3)	−21.9	1.0 (6)	−21.9	0.4 (6)	−22.5	1.4 (2)
BSW	0.6[b]															

—: not analyzed; (n): total number of replicate analyses, for all tubes analyzed for a particular vent; 1σ: standard deviation for all of the values that were averaged together to give a value for a particular vent.

[a] The reported $\delta^{13}C$ is the value calculated for the endmember hydrothermal vent fluid, assuming two-component mixing between a seawater endmember containing 2.33 mmol/kg CO_2, with a $\delta^{13}C$ of −0.6‰ and the endmember vent fluid with the calculated CO_2 concentration reported in Table 2. See text for discussion.

[b] Sansone et al. (1998).

averaged to give a single carbon isotopic composition for the different compounds for each vent (Table 3).

3. Results

Thirty fluid samples were collected from chimneys and spires at the Dead Dog and ODP Mound vent fields (Tables 1 and 2, Figs. 2 and 3). Figs. 2 and 3 indicate that there are large differences in fluid composition between Dead Dog and ODP Mound, while within each field, the fluids have a relatively narrow compositional range. Butterfield et al. (1994a) observed a similar trend for inorganic aqueous species. The lack of intrafield variation indicates that the entire vent field is fed by a common source region.

Measured vent fluid temperatures varied from 187 to 281 °C at Dead Dog and 263 to 272 °C at the ODP Mound field (Table 1). Similar temperatures were observed at these vents in 1990 (Butterfield et al., 1994a). A maximum temperature of 40 °C was measured for fluids venting from drillhole 1035F and 10 °C at drillhole 1035G. The fluid samples collected from drillhole 1035F have Mg concentrations between 43 and 48 mmol/kg (Table 1). Given the high degree of uncertainty associated with the calculated endmember compositions for this vent, especially for the volatile species since only one gas-tight sample was obtained, the data are reported in Tables 1 and 2, but are not discussed further. At Puppy Dog vent, diffuse flow exiting from around a low (~0.5 m high) mound covered with tube worms yielded a measured temperature of 17 °C. Upon removal of the worms, however, a discrete orifice was exposed in the sediment which yielded a measured temperature of 202 °C. Despite its relatively low temperature and isolated occurrence approximately 800 m south of the southern edge of the Dead Dog vent field, the composition of Puppy Dog vent fluids is similar to those at Dead Dog suggesting that they share a common source. Accordingly, Puppy Dog is included as part of the Dead Dog vent field in the subsequent discussion.

Owing to mixing of cold seawater during upflow in near seafloor environments, conductive cooling during upflow, and technical difficulties associated with positioning a thermocouple in the small region of hottest flow within a small chimney orifice, measured temperatures may not accurately reflect maximum subsurface temperatures in subsurface environments. The recurrence of maximum temperatures of 270 to 280 °C in many vents, however, suggests that these values do accurately reflect endmember fluid temperatures not affected by seawater mixing during measurement.

3.1. Inorganic aqueous species

Endmember ΣNH_3 concentrations are elevated in fluids from the Dead Dog field relative to fluids from the ODP Mound field. Endmember ΣNH_3 concentrations range from 2866 to 3020 μmol/kg in Dead Dog fluids and 2096 to 2340 μmol/kg fluid in fluids from Spire, Shiner Bock, and 1035H.

Aqueous H_2 concentrations for the Dead Dog fluids range between 1.9 and 2.6 mmol/L fluid, while at the ODP Mound field the concentrations ranged from 2.1 to 8.2 mmol/mL. Endmember CO_2 concentrations at Dead Dog (8.2 to 12 mmol/kg fluid) are, in general, lower than at the ODP Mound (8.2 to 13 mmol/kg fluid), although there is some degree of overlap (Fig. 2).

Chloride concentrations are quite distinct for the two vent fields. Concentrations in fluids from the Dead Dog field range between 546 and 586 mmol/kg fluid, while at the ODP Mound field, concentrations are depleted relative

to seawater, ranging from 432 to 449 mmol/kg fluid (Table 1). Chloride depletions in the ODP Mound fluids have been previously attributed to phase separation in the subsurface (Butterfield et al., 1994a).

3.2. Organic species

In general, the endmember abundances of saturated hydrocarbons are substantially higher in the Dead Dog fluids relative to the ODP Mound fluids (Table 2; Fig. 3). For example, methane concentrations from the Dead Dog and ODP Mound fields range from 18.5 to 22.6 and 2.99 to 7.07 mmol/mL fluid, respectively. Ethane, propane and *n*-butane show a similar trend and are characterized by substantial decreases in abundance with increasing chain length (Fig. 4). *Iso*- and *n*-butane concentrations are roughly equal in the Dead Dog fluids, while in the ODP Mound fluids, n-C_4 concentrations are approximately three times higher than i-C_4 concentrations (Table 2; Fig. 4). Endmember ethene and propene concentrations are substantially lower than their corresponding *n*-alkanes, ranging between 3.8–30 and 3.7–41 nmol/kg fluid, respectively (Table 2).

Benzene is also enriched by an order of magnitude in the Dead Dog fluids relative to the ODP Mound fluids, with maximum concentrations of approximately 28 and 2.6 μmol/kg fluid, respectively. Toluene concentrations are 25 times greater in Dead Dog fluids than in ODP Mound fluids, with maximum concentrations of 6 and 0.2 μmol/kg fluid, respectively (Table 2; Fig. 4).

3.3. Carbon isotopic compositions

The $\delta^{13}C$ values of aqueous ΣCO_2 range from −20.7‰ to −27.8‰ in the Dead Dog fluids, and from −33.4‰ to −34.6‰ in the ODP Mound fluids (Fig. 5). This range of

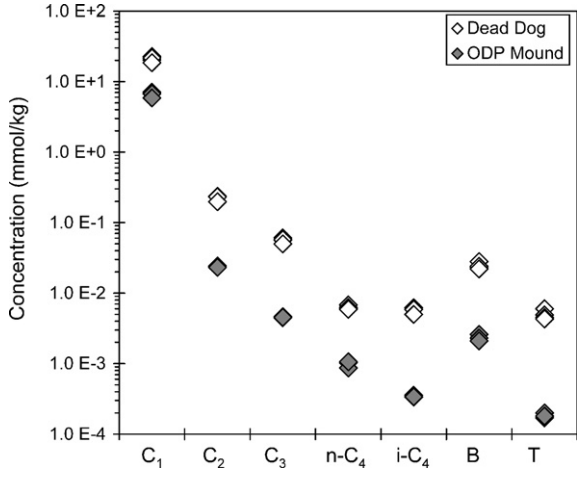

Fig. 4. Endmember concentrations of the low-molecular weight hydrocarbons in Middle Valley vent fluids. C_1: methane; C_2: ethane; C_3: propane; i-C_4: *iso*-butane; n-C_4: *n*-butane; B: benzene; T: toluene. Note the log scale. Because of the high uncertainty associated with the calculated endmember composition, the data for 1035F is not shown.

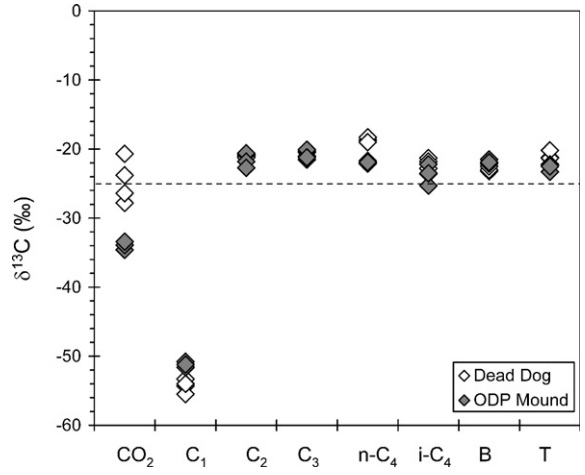

Fig. 5. Isotopic composition of aqueous carbon dioxide and low-molecular weight organic compounds in Middle Valley vent fluids. C_1: methane; C_2: ethane; C_3: propane; i-C_4: *iso*-butane; n-C_4: *n*-butane; B: benzene; T: toluene. The dashed line indicates the isotopic composition of sedimentary bitumen from the Dead Dog field (−24.9‰; Simoneit et al., 1992). Because of the high uncertainty associated with the calculated endmember composition, the isotopic composition of CO_2 for 1035F is not shown.

$\delta^{13}C$ values is consistent with, but narrower than, the range of −10.6‰ to −8.9‰ reported previously for aqueous CO_2 in Middle Valley vent fluids by Taylor (1992), although it is unknown whether the latter values are corrected for entrainment of seawater entrainment during sampling. Aqueous methane $\delta^{13}C$ values range between −53.3‰ and −55.5‰ at Dead Dog and −50.8‰ and −51.6‰ at ODP Mound. The isotopic composition of ethane, propane, and *iso*-butane in the Dead Dog and ODP Mound fluids are very similar, ranging between −20.1‰ and −25.3‰. *n*-Butane in the Dead Dog fluids is enriched in ^{13}C compared to both C_2–C_3 alkanes and i-C_4, ranging between −18.3‰ and −19.0‰. Within the accuracy of our measurements, the $\delta^{13}C$ of benzene and toluene in the ODP Mound fluids are identical to that for the C_2–C_4 alkanes, ranging between −21.5‰ and −22.5‰ and −22.2‰ to −24.4‰, respectively. In the Dead Dog fluids, the $\delta^{13}C$ of benzene ranges between −22.5‰ and −23.2‰, while the $\delta^{13}C$ of toluene ranges between −20.2‰ and −22.3‰. $\delta^{13}C$ values for aqueous aromatic compounds are similar to hydrothermal bitumen generated during hydrothermal sediment alteration at Middle Valley (Fig. 5; Simoneit et al., 1992).

4. Discussion

4.1. Sources of carbon compounds

Methane in sedimentary environments is typically classified as either "biogenic" or "thermogenic" based on its stable carbon isotopic composition and the relative abundances of co-existing longer-chained hydrocarbons (Schoell, 1980, 1988; Rice and Claypool, 1981; Welhan,

1988; Whiticar, 1999). Methane formed by heterotrophic and autotrophic microorganisms is characterized by a large range of $\delta^{13}C$ values (−42‰ to −105‰) that vary with community structure, metabolic pathway and environmental variables such as temperature (Schoell, 1988; Whiticar, 1999). Thermogenic methane formed from the abiogenic alteration of sedimentary organic matter at elevated temperatures typically has an isotopic composition between −25‰ and −50‰. Sedimentary basins influenced by magmatic activity or deep-seated mantle degassing may also contain mantle derived methane with $\delta^{13}C$ values between −20‰ to −10‰ (Des Marais et al., 1981; Welhan, 1988; Sherwood Lollar et al., 1993; Kelley and Früh-Green, 1999). Relative to biogenic and mantle-derived CH_4, which are accompanied by low concentrations of C_{2+} hydrocarbons, thermogenic gas may contain substantial concentrations of longer-chained *n*-alkanes. Thermogenic long-chained hydrocarbons from natural environments and from laboratory pyrolysis experiments are enriched in ^{13}C relative to co-existing methane. The extent of enrichment increases with chain length. Values of $\delta^{13}C$ for ethane and propane typically range between −18‰ and −34‰, with propane 5‰ to 8‰ heavier than ethane (Des Marais et al., 1988; Berner et al., 1995; Rooney et al., 1995; Lorant et al., 1998). The isotopic ratios of thermogenic methane, ethane and propane typically increase with increasing maturity of the source material (Berner et al., 1995; Lorant et al., 1998, and references therein; Rooney et al., 1995; Sherwood Lollar et al., 2002).

The isotopic composition of methane in vent fluids from Middle Valley varies between −50.8‰ and −5.5‰, (Table 3) and indicates that the mantle is not a significant source. Assessing the relative contribution of biogenic and thermogenic methane to Middle Valley fluids is more difficult because the measured ^{13}C contents fall within the ranges observed for both sources. The presence of hydrothermal activity, organic carbon-bearing sediments and abundant C_{2+} hydrocarbons with a ^{13}C content typical of thermogenic compounds (∼−20‰), provides evidence for a contribution of thermogenic methane to vent fluids at Middle Valley. The large ^{13}C depletions for methane relative to the C_{2+} hydrocarbons (Fig. 5), however, are consistent with the presence of significant microbial methane, suggesting that aqueous methane is mixture of both microbial and thermogenic inputs. Free gases recovered from sediments at Site 858 (Bent Hill) and Site 856 (Dead Dog) during ODP Leg 139 are characterized by isotopic compositions that are virtually identical to those reported here (Whiticar et al., 1994). Whiticar et al. (1994) estimated that between 60% and 85% of the methane in pore fluid samples is derived from bacterial sources, although this result is highly dependent on assumed values of −55‰ and −38‰ for the carbon isotope compositions of the endmembers. The presence of biogenic methane in Middle Valley vent fluids suggests that microbial processes in regions of the recharge zone where temperatures are sufficiently low to permit life (⩽∼121 °C; Stetter et al., 1990; Pledger and Baross, 1991; Blochl et al., 1997; Kashefi and Lovley, 2003) may significantly influence the composition of high temperature vent fluids.

While biogenic methane sources are confined to low temperature recharge zones, the release of organic compounds to solution during hydrothermal sediment alteration can occur during recharge, in deep-seated high temperature reaction zones, and during return flow to the seafloor. Hole 858G, drilled at the Dead Dog field (Fig. 1B), was cased through the sediment section and terminated in basaltic basement (Shipboard Scientific Party, 1992). High concentrations of B and NH_3 measured in pore fluids recovered from the bottom of the hole five years later during ODP Leg 169 indicate that hydrothermal fluids are interacting with sediments during both recharge and in deep-seated reaction zones (Shipboard Scientific Party, 1998b).

While the Dead Dog fluids are enriched in methane relative to the ODP Mound fluids, the opposite is observed for aqueous ΣCO_2 (Table 1, Figs. 2D and 3A). Carbon dioxide is unique among the carbon-containing aqueous species in that its abundance and isotopic composition is controlled not only by the alteration of sedimentary organic matter and magmatic degassing, but also by the precipitation and dissolution of carbonate minerals. Carbonate minerals formed during early diagenesis are typically characterized by $\delta^{13}C$ values near ∼0‰, but may approach values as low as −50‰ in low temperature sedimentary envronments where microbial methane oxidation occurs (Coleman et al., 1981). Because sedimentary organic matter is depleted in ^{13}C relative to seawater carbonate, CO_2 generated from the high temperature alteration of sedimentary organic matter will be significantly depleted relative to CO_2 derived from sedimentary inorganic carbonate sources alone (Krouse et al., 1988). The $\delta^{13}C$ of ΣCO_2 in fluids from both vent fields is low relative to magmatic values (−2‰ to −10‰, Shanks, 2001), ranging between −20.7‰ to −26.4‰ at the Dead Dog field, and −33.4‰ to −34.6‰ at the ODP Mound field (Table 3; Fig. 5).

The relatively depleted $\delta^{13}C$ compositions of aqueous ΣCO_2 suggest that its main source is the hydrothermal alteration of sedimentary organic matter. This may involve generation directly from oxygen-bearing functional groups or from the oxidation of previously generated hydrocarbons. For example, the carbon in aqueous CH_4 can be oxidized to CO_2 as follows (Seewald, 1994):

$$CH_{4(aq)} + 2H_2O = CO_{2(aq)} + 4H_{2(aq)} \quad (3)$$

Degradation of longer-chained *n*-alkanes under hydrothermal conditions occurs via a stepwise oxidation reaction mechanism that ultimately results in the production of both CO_2 and CH_4 (Seewald, 2001a). In general, the overall process can be represented by the net reaction:

$$\underset{n\text{-butane}}{C_4H_{10(aq)}} + 4H_2O = 2CO_{2(aq)} + 2CH_{4(aq)} + 5H_{2(aq)} \quad (4)$$

Note that although the carbon in CH_4 produced by this reaction is in a more reduced state than in butane, there is a net oxidation of the total carbon as butane (or any alkane)

is consumed due to the production of oxidized carbon in CO_2. Reaction (4) differs from the disproportionation reaction ($C_4H_{10(aq)} + 3/2\ H_2O = 13/4\ CH_{4(aq)} + 3/4\ CO_{2(aq)}$) because aqueous hydrogen is produced from the reduction of water. Aqueous H_2 generated during the oxidation of aqueous hydrocarbons has important implications for the redox state of hydrothermal fluids. Measured H_2 concentrations at Middle Valley are substantially higher than can be produced by fluid-basalt interaction (Seyfried and Ding, 1995) and suggest a critical role for sedimentary organic matter. It is evident from the stoichiometry of reactions (3) and (4) that hydrocarbon oxidation represents a particularly effective means for the generation of H_2. Depending on the minerals present in the system, even greater amounts of H_2 can be produced per mole of alkane oxidized (Seewald, 2001a,b). Thus, aqueous H_2 concentrations that range from 1.9 to 8.2 mmol/L in high temperature Middle Valley vent fluids, are consistent with extensive organic matter oxidation in the subsurface. The presence of more ^{13}C depleted CO_2 along with higher H_2 and CO_2 abundances in ODP Mound fluids relative to Dead Dog suggests oxidation reactions have proceeded to a greater extent at the ODP Mound.

The ^{13}C-depleted CO_2 in Middle Valley vent fluids might alternatively be produced by anaerobic methane-oxidizing microorganisms in recharge zones. This scenario requires an initial transition from sulfate-rich pore fluids to a sulfate-free environment that would allow the formation of microbial CH_4, followed by the reappearance of sulfate at depth to act as an electron acceptor during anaerobic CH_4 oxidation. Elevated SO_4 concentrations in deep pore fluids and the presence of anhydrite at depth in Middle Valley sediments (Shipboard Scientific Party, 1998a) suggest that such transitions are feasible. Microbial anaerobic CH_4 oxidation cannot account for the exceptionally high aqueous H_2 concentrations observed in these fluids. However, formation of mmolal abundances of aqueous H_2 by the net oxidation of organic matter also results in the formation of mmolal concentrations of ^{13}C-depleted CO_2, consistent with the hypothesis that aqueous ΣCO_2 in Middle Valley vent fluids is largely derived from abiogenic, hydrothermal alteration of organic matter.

In addition to CH_4 and CO_2, hydrothermal sediment alteration releases other organically derived compounds. Elevated alkane, aromatic and ΣNH_3 concentrations in the Dead Dog fluids compared with the ODP Mound fluids likely reflect differences in the amount of fresh sediment encountered by fluids in the subsurface. Differences in the extent of fluid–sediment interaction can be assessed by calculating fluid:sediment mass ratios using measured aqueous ΣNH_3 concentrations and assuming that nitrogen is quantitatively removed from the sediments during alteration. This approach is supported by laboratory experiments that demonstrate near quantitative release of ΣNH_3 to solution at temperatures above 200 °C (Seewald et al., 1994). Unaltered Middle Valley sediment typically contains ~0.06 wt.% N (Goodfellow and Peter, 1994), resulting in calculated fluid:sediment mass ratios of ~14 for Dead Dog fluids and 18–20 for the ODP Mound fluids. These values suggest that the amount of sediment–fluid interaction at the ODP Mound field is slightly less than that at the Dead Dog field. This may be due to differences in the age of the two vent fields, whereby longer-lived venting at the ODP Mound has resulted in decreased availability of fresh nitrogen-bearing sediments relative to the Dead Dog field. Alternatively, varying fluid:sediment mass ratios could reflect flow path differences in the recharge and reaction zones for both fields.

4.2. Reaction zone conditions

As seawater circulates through the crust and undergoes progressive heating and reaction with basement rocks or sediments, the point of maximum heating is often referred to as the "reaction zone" (Alt, 1995). Commonly, this is thought of as occurring at the point of deepest circulation prior to the fluid returning to the seafloor. The composition of vent fluids reflects the integrated effects of chemical reactions occurring over a broad range of temperatures along the entire flowpath. We can constrain minimum pressures in the highest temperature reaction zones at Middle Valley if it is assumed that maximum fluid temperatures are attained in within the basaltic basement rocks that represent the heat source for hydrothermal activity. Water depth at both vent fields is 2400 m. Thus, at Dead Dog, 260 m of overly sediment corresponds to minimum pressures of 260 bar in the basaltic basement. At the ODP Mound, 400 m of overlying sediment increases minimum basement pressures to 280 bar. Golden et al. (2003) have interpreted microseismicity located 1.5 km beneath the seafloor at the Dead Dog field as the product of a cracking front that results from the penetration of relatively cool fluids into hot rock (Lister, 1974, 1983). The presence of a cracking front at 1.5 km beneath the seafloor constrains maximum pressures to 390 bar.

Estimating fluid temperatures in the reaction zone can be more problematic because fluid temperatures measured at the seafloor may be significantly lower than reaction zone conditions due to subsurface mixing and conductive and adiabatic heat-loss during upflow (Seyfried et al., 1988; Seewald and Seyfried, 1991). Geothermometers based on the abundance of aqueous inorganic species such as Cl, Si, transition metals and Na/Ca ratios have been used in the past to estimate reaction zone temperatures in unsedimented ridge-crest hydrothermal systems (Von Damm et al., 1985; Seewald and Seyfried, 1991; Seewald et al., 2003; Seyfried et al., 2003). In regions such as Middle Valley where hydrothermal fluids also interact with organic-carbon containing sediments, organic compounds may serve as geochemical proxies to provide further insight into subsurface temperature regimes and hydrology.

4.2.1. Kinetic constraints

During the thermal alteration of sedimentary organic matter, the relative abundances of low molecular weight

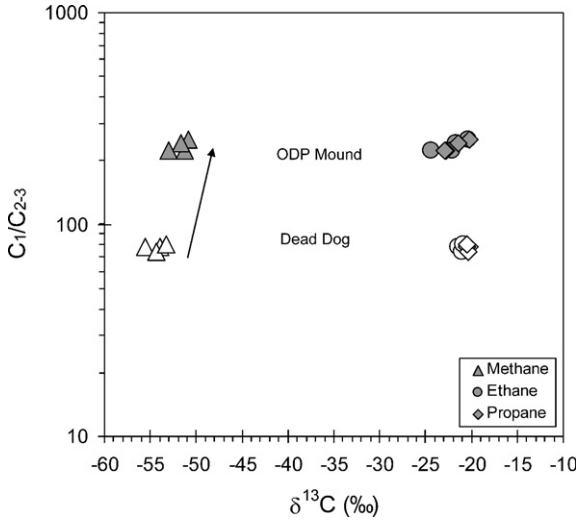

Fig. 6. $C_1/(C_2 + C_3)$ versus $\delta^{13}C$ (‰) for aqueous methane, ethane and propane in Dead Dog (white symbols) and ODP Mound (gray symbols) fluids. The arrow indicates the observed trend for increasing extent of reaction among aqueous organic compounds in the subsurface. Because of the high uncertainty associated with the calculated endmember composition, the data for 1035F is not shown.

n-alkanes can be used as a maturation indicator. With increasing thermal stress, the relative abundance of methane increases due to degradation reactions (i.e. reaction (4)) that transform longer chain hydrocarbons to shorter chain products (Tissot and Welte, 1984; Hunt, 1996). The ODP Mound fluids are characterized by $C_1/(C_2 + C_3)$ ratios near 245, while the Dead Dog fluids have ratios near 70 (Table 2, Fig. 6). This difference suggests that ODP Mound fluids have attained higher levels of thermal stress. The degradation of straight chain hydrocarbons that constitute petroleum is generally viewed as a kinetically controlled process, where time and temperature are interchangeable variables (Braun and Rothman, 1975; Tissot and Welte, 1984; Waples, 1984; Burnham et al., 1995; Hunt, 1996). Thus, higher $C_1/(C_2 + C_3)$ ratios at the ODP Mound relative to Dead Dog indicate a more mature hydrocarbon suite that, in turn, reflects higher subsurface temperatures and/or longer subsurface residence times for circulating fluids.

The relative abundances of butane isomers also suggest higher thermal maturities for hydrocarbons at ODP Mound compared with the Dead Dog vent field. With increasing maturation, degradation of longer chain hydrocarbons leads to a predominance of straight-chained alkanes over their branched counterparts (Hunt et al., 1980; Whelan et al., 1988; Hunt, 1985). Thus, increases in the n-C_4:i-C_4 ratio from a value of ~1 in the Dead Dog fluids to 2.6–3.0 in the ODP Mound fluids are consistent with greater thermal stress at the ODP Mound field.

Measured aqueous Cl concentrations can constrain the relative influence of time and temperature during organic alteration processes. Aqueous Cl concentrations in the Dead Dog fluids are enriched relative to seawater by a maximum of only 8% (Fig. 2A). Such enrichment can be attributed to hydration reactions during sediment and basalt alteration. In contrast, the ODP Mound fluids have Cl concentrations that are depleted relative to seawater by 17–20% (Fig. 2A). Because Cl is a conservative species during water–rock reactions at temperature conditions typical of ridge-crest hydrothermal systems, vent fluid Cl depletions are generally attributed to subsurface phase separation (Lilley et al., 1993; Butterfield et al., 1994b; Von Damm et al., 1995; Seewald et al., 2003; Seyfried et al., 2003). At seafloor pressures of 240 bar, fluid temperatures of at least 385 °C are required to cause phase separation of seawater–chlorinity fluids, with higher temperatures required at greater depths (Fig. 7). Phase separation has also been identified as a key process regulating fluid compositions in other sedimented seafloor systems, such as Escanaba Trough (Von Damm et al., 2005). Accordingly, chloride-depleted fluids at ODP Mound indicate that reaction zone temperatures must exceed 385 °C. Measured exit temperatures ⩽272 °C indicate that fluids venting at the ODP Mound field have cooled by at least 120–145 °C during flow from the hottest region of the subsurface reaction zone to the seafloor. Assuming similar depths of circulation at the Dead Dog field, the absence of phase separated fluids

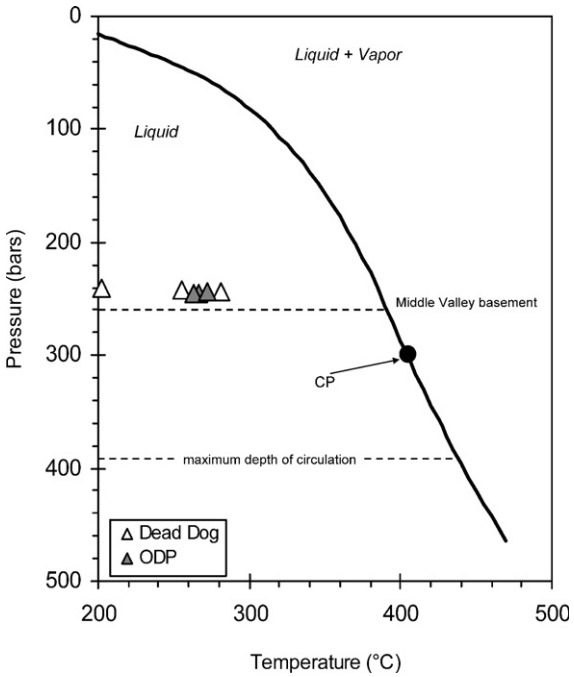

Fig. 7. Two-phase diagram for seawater (3.2 eq. wt. % NaCl) redrawn from Bischoff and Rosenbauer (1985). The measured exit temperatures and pressures for the sampled vents are indicated with triangles. At seafloor conditions of 240 bar and measured fluid temperatures, all of the vents are within the single phase region. This indicates that significant cooling must have occurred in the ODP Mound fluids during ascent to account for endmember Cl concentrations that are less than seawater values. CP: critical point for seawater. Lines drawn at 260 bar represent minimum depths to basaltic basement at Middle Valley. Line drawn at 390 bar represents maximum fluid circulation depth of ~1.5 km (Golden et al., 2003).

indicates that the reaction zone must be cooler than at the ODP Mound field. Higher reaction zone temperatures at ODP Mound compared with Dead Dog are consistent with the higher $C_1/(C_2 + C_3)$ ratios at this location. This result suggests that temperature, rather than fluid residence time, may be the dominant variable regulating the relative abundances of low molecular weight hydrocarbons in these fluids. While phase separation may affect the absolute abundances of organic compounds in the liquid phase, the relative abundances of organic species in the liquid phase will record subsurface conditions if thermodynamic reequilibration occurs following phase partitioning.

The chemical processes that control the relative distributions of *n*-alkanes derived from organic matter alteration also affect their stable carbon isotopic composition. Comparison of fluids from both vent sites indicates that higher $C_1/(C_2 + C_3)$ ratios in the ODP Mound fluids are accompanied by ^{13}C-enriched methane relative to the Dead Dog fluids (Fig. 6). This trend suggests that a greater fraction of the dissolved methane at the ODP Mound is derived from hydrothermal degradation of relatively ^{13}C-enriched longer chain hydrocarbons. Collectively, the heavier $\delta^{13}C$ of methane and higher $C_1/(C_2 + C_3)$ ratios in the ODP Mound fluids relative to the Dead Dog fluids are consistent with the hypothesis that the subsurface below the ODP Mound field is hotter than at the Dead Dog field.

In contrast to the observed shift in methane isotopic compositions, the $\delta^{13}C$ of the C_2–C_4 of aqueous alkanes lie in a narrow range between $-18‰$ and $-23‰$, with little to no difference between the two fields (Table 3, Fig. 5). In general, differences in the isotopic composition of individual low molecular weight thermogenic alkanes decreases with increasing thermal maturity (James, 1983). Near constant $\delta^{13}C$ values for C_2–C_4 hydrocarbons at Middle Valley indicate high levels of thermal maturity, consistent with high temperature reaction zones. Moreover, the isotopic composition of ethane and propane in natural gases from economic petroleum accumulations that have experienced extensive thermochemcial sulfate reduction have been shown to converge on a single $\delta^{13}C$ value (Krouse et al., 1988). Thus, the uniformity of $\delta^{13}C$ values for C_2–C_4 hydrocarbons at Middle Valley may indicate that reactions responsible for the oxidative degradation of hydrocarbons (i.e. reaction (4)) are analogous to oxidative processes occurring in petroleum reservoirs.

4.2.2. Equilibrium constraints

Although the absolute abundances of low molecular weight alkanes in Middle Valley vent fluids reflect the extent of kinetically controlled decomposition reactions, the relative abundance of other aqueous organic compounds may attain a state of thermodynamic equilibrium if suitable reaction paths are available. In contrast to kinetic processes that respond to time, temperature, and the chemical composition of the system, reactions that attain thermodynamic equilibrium are time invariant and regulated solely by temperature, pressure, and chemical composition. While the absolute abundances of volatile species can be affected by phase separation, the relative abundances will record subsurface conditions when compounds reequilibrate following phase partitioning (see below).

4.2.2.1. Alkane–alkene equilibria. Laboratory experiments designed to investigate the interaction of organic compounds with water and minerals at elevated temperatures and pressures in natural environments demonstrated that the relative abundances of aqueous alkenes and alkanes may be regulated by redox-dependent metastable equilibria (Seewald, 1994, 1997, 2001a). Equilibration of ethene–ethane and propene–propane concentrations can be represented by the reactions:

$$\underset{\text{ethene}}{C_2H_{4(aq)}} + H_{2(aq)} = \underset{\text{ethane}}{C_2H_{6(aq)}} \quad (5)$$

$$\underset{\text{propene}}{C_3H_{6(aq)}} + H_{2(aq)} = \underset{\text{propane}}{C_2H_{8(aq)}} \quad (6)$$

Because the equilibrium constant (K_{eq}) varies systematically as a function of temperature, the measured composition of Middle Valley vent fluids can be used to constrain reaction zone temperatures if pressure can be independently constrained. Equilibrium according to reactions (5) and (6) in Middle Valley vent fluids represents a metastable state because ethane, ethane, propane, and propene are thermodynamically unstable and should react to produce CO_2 and CH_4 in the absence of kinetic barriers. To allow calculation of subsurface temperatures, a pressure of 350 bar was assumed for subsurface reaction zones at the Dead Dog and ODP Mound fields. This value is bracketed by the minimum and maximum estimates of subsurface pressure conditions. However, the assumption of pressure has little effect on calculated temperatures because the equilibrium positions of these reactions are relatively insensitive to pressure over the 150 bar range constrained by the depth of the seafloor (240 bar) and magma chambers (390 bar) at Middle Valley. Values of K_{eq} for reactions (5) and (6) were calculated from thermodynamic data compilation of Johnson et al. (1992, and references therein). Activity coefficients for the neutral species involved in this reaction species were assumed to be unity.

Temperatures estimated for ethane–ethene equilibration at the Dead Dog field vary from 336 to 364 °C while those at the ODP Mound vary from 405 to 418 °C (Table 4, Fig. 8). In general, the absolute temperatures estimated assuming propene–propane equilibrium are lower than for ethene–ethane equilibrium, varying from 305 to 345 °C and 362 to 383 °C at the Dead Dog and ODP Mound fields, respectively. The cause of this difference is presently unclear, but may reflect a lack of equilibrium due to competing reactions that consume propene faster than it can be produced by propane oxidation (Seewald, 2001a). Temperatures estimated from the Dead Dog fluids are marginally hotter than the ~270–300 °C estimated for the basement at the Dead Dog field using models based the sediment physical properties, heat flow measurements,

Table 4
Reaction zone temperatures (°C) at Middle Valley, estimated from different chemical proxies for 350 bar pressure

Vent	Cl[a]	Ethene–ethane[b]	Propene–propane[b]	Benzene–toluene[b]	CO_2–CH_4[b]	$\delta^{13}C$, CO_2–CH_4[c]
Dead Dog						
Heineken Hollow	<422	336	345	253	299	275
Chowder Hill	<422	344	305	261	310	225
Inspired Mounds	<422	364	331	262	308	190
Puppy Dog	<422	339	—	255	302	255
ODP Mound						
1035F	⩾422	418	383	263	319	250
Shiner Bock	⩾422	410	376	304	360	450
Spire	⩾422	405	362	270	317	425
1035H	⩾422	413	378	294	351	420

[a] Temperature of two-phase boundary for seawater at 350 bar (Bischoff and Rosenbauer, 1985).
[b] Minimum temperature for phase separation at estimated reaction zone depth. Based on assumed attainment of chemical equilibrium according to reactions (3), (5)–(7).
[c] Based on assumed attainment of isotopic equilibrium.

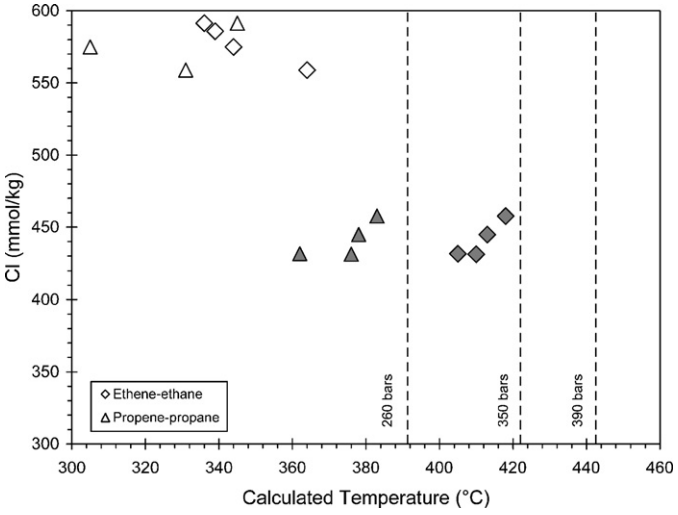

Fig. 8. Equilibration temperatures calculated for ethene:ethane (triangles) and propene:propane (diamonds) redox couples versus endmember Cl concentrations in Dead Dog (white symbols) and ODP Mound (gray symbols) vent fluids. For reference, the two-phase boundary for seawater at 260 bar (representing minimum reaction zone temperature), 350 bar (pressure used in calculation) and 390 bar (maximum pressure of reaction zone) are indicated by dotted lines.

the geochemistry and mineralogy of altered basaltic sills at ODP Site 857 and trapping temperatures of fluid inclusions from ODP Sites 858 and 857 (Davis and Villinger, 1992; Davis and Wang, 1994; Peter et al., 1994; Stakes and Schiffman, 1999). Lower calculated temperatures for the Dead Dog field fluids relative to the ODP Mound field are also consistent with differences in alkane abundances and the isotopic composition of aqueous methane (Fig. 6).

Temperatures estimated from alkane–alkene equilibria are also consistent with vent fluid Cl abundances (Table 3). Measured Cl concentrations in fluids from these two fields indicate that maximum subsurface temperatures were sufficiently high to induce phase separation at the ODP Mound, but not at the Dead Dog field. Indeed, temperatures calculated for ethene–ethane equilibrium in the ODP Mound fluids are close to the phase boundary for seawater at 350 bar (Fig. 8). The lower calculated temperatures for the Dead Dog fluids place them in the single phase region for seawater, consistent with the absence of a chloride depletion. The estimated subsurface temperatures at both locations based on alkane–alkene equilibria are significantly higher than maximum measured exit temperatures of approximately ~270 °C, suggesting that the fluids have cooled to varying degrees in the subsurface prior to venting.

4.2.2.2. Benzene–toluene equilibria. Consistent with the higher alkane, alkene and ΣNH_3 concentrations in the Dead Dog fluids, benzene and toluene are also enriched in Dead Dog fluids compared with ODP Mound fluids (Table 2; Fig. 4C). Although benzene concentrations are greater than toluene concentrations in all fluids, benzene:toluene ratios are higher in the ODP Mound fluids than in the Dead Dog fluids, ranging between 11 to 13.5 and 4.6 to 5.3, respectively (Table 2). Although benzene is highly stable in high temperature geologic environments, McCollom et al. (2001) demonstrated that toluene may be degraded under hydrothermal conditions according to the reaction:

$$\underset{\text{toluene}}{C_6H_5CH_{3(aq)}} + 2H_2O \rightarrow \underset{\text{benzene}}{C_6H_{6(aq)}} + CO_{2(aq)} + 3H_{2(aq)} \qquad (7)$$

The availability of thermodynamic data for reaction (7) in the compilation of Johnson et al. (1992, and references therein) allows temperatures to be estimated from the measured fluid chemistry, again assuming the attainment of metastable thermodynamic equilibrium and a pressure of 350 bar. These calculations yield estimated temperatures of 253–262 °C at the Dead Dog field and 263–304 °C at the ODP Mound field (Table 4). With the exception of the Heineken Hollow and Puppy Dog vents, where measured exit temperatures are lower than estimated subsurface temperatures, the measured benzene:toluene ratios are consistent with equilibrium at the measured exit temperatures at the Dead Dog field (Fig. 9). Although there is a slight indication of higher temperatures at ODP

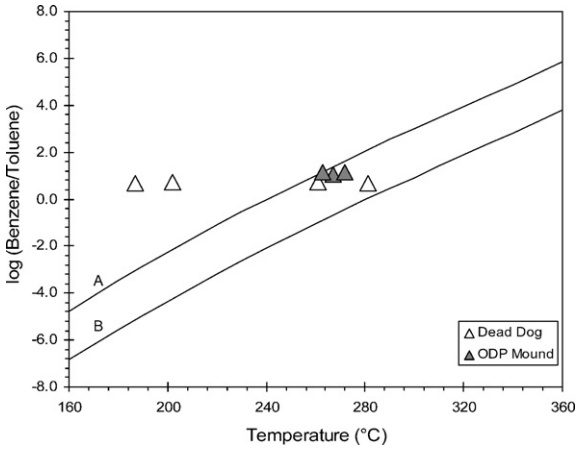

Fig. 9. Measured values of log(benzene/toluene) versus measured exit temperature for Dead Dog (white triangles) and ODP Mound (gray triangles) fluids. Solid lines indicate the range of log(benzene/toluene) values calculated according to reaction (7) at 350 bar using data in the SUPCRT92 database (Johnson et al., 1992 and references therein), and aqueous H_2 and CO_2 concentrations that bracket those measured in the vent fluids (A: $H_2 = 1.9$ mmol/kg fluid, $CO_2 = 8.2$ mmol/kg fluid; B: $H_2 = 8.2$ mmol/kg fluid, $CO_2 = 12$ mmol/kg fluid).

Mound, the temperature estimates are also very similar to the measured vent temperatures. Therefore, in contrast to alkene–alkane equilibria, benzene and toluene concentrations do not appear to record maximum reaction zone conditions.

4.2.2.3. Methane–carbon dioxide equilibria. Temperatures can also be estimated from measured concentrations of CO_2, CH_4, and H_2 using thermodynamic data for reaction (3). In this case, however, the assumption of thermodynamic equilibrium may be more tenuous since the kinetics associated with the reduction of CO_2 to CH_4 are known to be quite slow (Schofield, 1973; Barnes, 1981). Previous work with other natural and experimental hydrothermal systems have demonstrated that equilibrium between CH_4 and CO_2 may not be attained at temperatures characteristic of ridge-crest hydrothermal systems (Arnórsson and Gunnlaugsson, 1985; Janecky et al., 1986; Welhan, 1988). However, hydrothermal alteration experiments using organic-rich sediment from Guaymas Basin indicate that thermodynamic equilibrium can be attained between aqueous CO_2 and CH_4 at ridge-crest temperatures (Seewald et al., 1994). Thus, whether chemical equilibrium is achieved according to reaction (3) may depend on the direction from which equilibrium is approached. While the reaction rates in both the forward and reverse direction must be the same at equilibrium, they need not be identical when the system is far removed from equilibrium. Therefore, in organic-poor systems, an approach to equilibrium from a state of excess CO_2 may be inhibited by sluggish reaction kinetics for CO_2 reduction (Schofield, 1973; Barnes, 1981). In contrast, in sedimented systems characterized by excess thermogenic CH_4, rapid reaction kinetics may facilitate the attainment of near equilibrium states (Seewald et al., 1994).

Equilibration of CO_2 and CH_4 at the temperature and pressure conditions in the hottest regions of the reaction zone requires the reaction of CH_4 to form CO_2 and H_2 based on the thermodynamic data for reaction (3). Estimated temperatures assuming CO_2–CH_4 equilibrium at 350 bar range between 299–308 and 317–360 °C for the Dead Dog and ODP Mound fields, respectively (Table 4). Higher calculated temperatures for ODP Mound compared with the Dead Dog field are, again, consistent with temperature estimates based on other geochemical indicators. These values, however, are intermediate between the high temperatures determined from the alkene–alkane geothermometer and Cl concentrations, and the low temperatures measured at the vents and calculated from benzene and toluene concentrations.

In addition to chemical equilibrium, aqueous CO_2 and CH_4 can also achieve carbon isotopic equilibrium. Based on the fractionation factors provided by Horita (2001), the isotopic compositions of coexisting CO_2 and CH_4 yield equilibrium temperatures that vary from 190 to 275 °C for the Dead Dog fluids and 425 to 450 °C for the ODP Mound fluids (Table 4). Values for the Dead Dog field are lower than the measured vent temperatures and temperatures estimated using other chemical proxies suggesting that CO_2 and CH_4 have not equilibrated isotopically. In contrast, values for the ODP Mound fluids are consistent with temperatures required for phase separation (422 °C at 350 bar). Although it is tempting to entertain the possibility that faster exchange kinetics associated with higher subsurface temperatures at the ODP Mound have facilitated isotopic equilibration of CO_2 and CH_4, attainment of isotopic equilibrium between CO_2 and CH_4 is estimated to be 100 times slower than attainment of chemical equilibrium in geothermal systems (Giggenbach, 1982; Kiyosu and Krouse, 1989). Thus, the agreement between temperatures calculated from the isotopic composition of CO_2 and CH_4 and temperatures required for phase separation in deep-seated reaction zones may simply be fortuitous.

4.3. Subsurface cooling processes

Differences in subsurface temperatures estimated using the chemical geothermometers discussed above can be used to constrain subsurface processes responsible for cooling of high temperature vent fluids at Middle Valley. Hydrothermal fluid temperatures may decrease during upflow in response to conductive heat loss to the surrounding crust or mixing with lower temperature hydrothermal fluids. Conductive heat loss in subsurface environments is not an efficient mechanism to cool hydrothermal fluids due to the low thermal conductivity of basaltic rocks and sediments (Sleep and Morton, 1983). From a chemical perspective, a conductive cooling model is not suggested for Middle Valley since it requires that the relative abundances of alkanes and alkenes formed at high temperature are quenched during cooling, while benzene and toluene

reequilibrate during upflow. This scenario is opposite to reaction kinetics observed during laboratory experiments where equilibration of low molecular weight alkanes and alkenes occurs rapidly at temperatures near 300 °C provided reduced sulfur species are present in the system (Seewald, 1997, 2001a), while benzene–toluene equilibration is significantly slower (McCollom et al., 2001). Moreover, the stability of alkenes relative to alkanes decreases with decreasing temperature indicating that reequilibration would require the reaction of only nmolal amounts of alkenes. In contrast, toluene stability increases with decreasing temperature such that a ~400 °C fluid containing insignificant quantities of benzene at equilibrium must generate μmolal quantities of toluene to reequilibrate at the measured vent temperatures. We therefore believe that conductive cooling within the crust is not responsible for fluid heat loss during ascent from high temperature reaction zones to the seafloor.

Subsurface mixing of a hydrothermal fluid reacted at high temperature with a second lower temperature hydrothermal fluid can have a significant impact on the chemistry and temperature of hydrothermal circulation. We postulate that such a process is occurring at both the Dead Dog and ODP Mound vent fields since it can account for the measured vent temperatures and fluid composition. Within the context of this model, mixing may occur at the millimeter scale in a "cracking front" as hydrothermal fluid that is rapidly heated upon exposure to fresh hot rock ascends and mixes with overlying fluid, or at a larger scale by conductive heating at the base of a hydrothermal reservoir. In both cases, the overlying lower temperature fluid represents the ultimate source of the high temperature fluid. Mixing of high temperature low salinity vapors with lower temperature, seawater–salinity hydrothermal fluids that represent the source of the vapors, has been suggested as an important process that regulates the temperature and composition of vent fluids at the Main Endeavour vent field (Seewald et al., 2003).

The effects of subsurface mixing on fluid composition and temperature at the ODP Mound can be demonstrated by mixing a hypothetical fluid formed at 250 °C and 350 bar with a hypothetical low salinity vapor formed at 440 °C (Table 5). The compositions of these fluids where chosen to demonstrate the effect of mixing on the relative abundances of aqueous organic compounds. For the purpose of these calculations we have used the composition of the Shiner Bock fluid (Tables 1 and 2) and assumed that the fractions of total carbon represented by $CO_2 + CH_4$, ethane + ethene, propane + propene, and toluene + benzene remain constant at each temperature condition. We have also assumed that all carbon species quantitatively partition into the vapor during phase separation at 440 °C. For the 250 °C fluid, CO_2, CH_4, and H_2 concentrations were assumed to be 10, 9.1, and 1.2 mmolal, respectively, and do not represent equilibrium abundances according to reaction (3). Using these values, metastable equilibrium abundances of alkanes and their corresponding alkenes, and benzene and toluene were calculated at 250 °C. The composition of the 440 °C fluid was calculated assuming phase separation at 350 bar and the removal of kinetic barriers to reaction (3) at the higher temperature, thereby allowing equilibration of CO_2 and CH_4. Due to the high abundance of CO_2 and CH_4 relative to the other carbon species, equilibration according to reaction (3) directly constrains the activity of aqueous H_2 in the high temperature fluid. These values were then used to calculate metastable equilibrium abundances of the low molecular weight hydrocarbons. The mixed fluid is composed of 80% of the 250 °C fluid and 20% of the 440 °C fluid, which corresponds to a temperature of 288 °C assuming constant heat capacity as a function of temperature. Because heat capacity increases with increasing temperature, the calculated temperature represents a minimum value.

Table 5
Mixing model to account for the composition of hydrothermal vent fluids at Middle Valley

	250 °C fluid	440 °C fluid	Mixed fluid	Shiner Bock
Mole fraction	0.8	0.2		
T (°C)	250	440	288	272
Cl (mM)	543	95[a]	453	448
H_2 (mM)	1.2	37	8.5	8.2
CO_2 (mM)	10	19	12	12
CH_4 (mM)	9.07	1.41E−06	7.3	7.1
$\log K_{CH_4\text{–}CO_2}$	−14.2	1.43		
Ethane (μM)	24	24	24	24
Ethene (nM)	0.0041	45	9.0	8.4
$\log K_{ethene\text{–}ethane}$[b]	9.69	4.16		
Propane (μM)	4.63	4.63	4.63	4.6
Propene (nM)	0.029	344	69	3.7
$\log K_{propene\text{–}propane}$[b]	8.12	2.56		
Benzene (μM)	2.6	2.8	2.6	2.6
Toluene (μM)	0.25	1.4E−09	0.20	0.20
$\log K_{benzene\text{–}toluene}$[b]	9.746	−3.311		

See text for individual reactions.
[a] From Bischoff and Pitzer (1989).
[b] Thermodynamic data are from the SUPCRT92 database (Johnson et al., 1992 and references therein).

Examination of Table 5 reveals that virtually every aspect of the Shiner Bock vent fluid at the ODP Mound can be accounted for by the mixing of these two hypothetical fluids, including the Cl concentration. In particular, the disparate temperature dependence of alkane–alkene equilibria and benzene–toluene equilibria allows these geothermometers to reflect temperatures in different regions of the reaction zone. For example, the concentrations of ethane and propane are identical at 250 and 440 °C, but the 440 °C fluid contains approximately 4 orders of magnitude more ethene and propene than the 250 °C fluid. Thus, even though the mixed fluid contains 80% of the low temperature endmember, the alkene abundance is dominated by the high temperature component. The inverse is true for benzene–toluene equilibria because toluene is more stable at lower temperatures. Accordingly, toluene concentrations in 250 °C fluid are 10 orders of magnitude higher than the

440 °C fluid, and dominate the composition of the mixed fluid. Although mixing influences the abundance of some species in the mixed fluid by up to a factor of 4, these variations are relatively minor when compared the to influence of order-of-magnitude changes in the equilibrium constant with temperature for alkene–alkane and benzene–toluene equilibria (Table 5). The variations in the K_{eq} values allow the mixed fluid to record both high and low temperature equilibrium compositions. The net result of mixing is that the alkane–alkene geothermometer slightly underestimates temperatures of phase separation and the benzene–toluene geothermometer slightly overestimates the temperature of the cool endmember fluid. A similar mixing calculation involving high and low temperature hydrothermal fluids can be used to account for the composition of the Dead Dog fluids, but the high temperature endmember will not have experienced phase separation. The hypothetical endmember fluid compositions used in the mixing model are by no means unique, but are intended only to demonstrate that the composition of vent fluids at Middle Valley are consistent with subsurface mixing of genetically related hydrothermal fluids.

5. Conclusions

Vent fluids from two areas of active hydrothermal activity at Middle Valley, the Dead Dog and ODP Mound fields, are enriched in a suite of aqueous organic compounds. The fluids from both fields interact extensively with sediments, which serve as a source of aqueous organic compounds. Methane is derived from bacterial sources during recharge and hydrothermal alteration of organic-bearing sediments during recharge and in subsurface reaction zones. Alteration of sedimentary organic matter also leads to the generation of longer-chained aqueous hydrocarbons and carbon dioxide Organically derived carbon dioxide may be generated directly from oxygen-bearing functional groups, or the secondary oxidation of aqueous hydrocarbons. Oxidation of hydrocarbons in vent fluids also impacts fluid redox. Higher concentrations of aqueous hydrogen in ODP Mound fluids compared with the Dead Dog fluids suggests oxidation reactions have proceeded to a greater extent at the ODP Mound. Lower ammonia concentrations in the ODP Mound fluids indicate less sediment–fluid interaction at the ODP Mound field as compared to the Dead Dog field.

Aqueous organic compounds in Middle Valley vent fluids can be used to constrain temperature conditions in deep-seated reaction zone conditions. Lower $C_1/(C_2 + C_3)$ and n-C_4:i-C_4 ratios in the Dead Dog fluids point to lower subsurface temperature conditions at the Dead Dog area compared with the ODP Mound. The isotopic composition of aqueous methane is also consistent with a hotter subsurface at the ODP Mound. Trends in the abundance and isotopic composition of aqueous organic species are consistent with: (1) depleted chloride concentrations in the ODP Mound fluids that point to hotter subsurface temperatures required for phase separation and (2) the absence of phase separation in the lower temperature, seawater–chlorinity Dead Dog fluids.

Temperatures estimated using alkane–alkene pairs and the assumption of metastable thermodynamic equilibrium indicate that the ODP Mound fluids have experienced subsurface temperatures of approximately 420 °C at the ODP Mound field and 350 °C at the Dead Dog field. In contrast, temperatures recorded by metastable benzene–toluene equilibrium are approximately 270 °C, and are generally consistent with measured exit temperatures. Temperatures calculated assuming carbon dioxide–methane equilibrium are intermediate between alkane–alkene and benzene–toluene equilibrium. In the case of the ODP mound, these differences point to subsurface mixing of the hottest vent fluids during ascent to the seafloor. Specifically, mixing of a phase separated vapor with a lower temperature, seawater–salinity hydrothermal fluid that is the source of the vapors, can result in a mixed fluid with an organic composition, chlorinity, and temperature that is very similar to venting fluids. This model implies that a high temperature vapor phase is currently forming at the ODP Mound field, but does not reach the seafloor due to subsurface mixing. The occurrence of minerals such as isocubanite and wurtzite in the ODP Mound massive sulfide deposit indicates precipitation from high temperature (>350 °C) vent fluids at the seafloor (Zierenberg et al., 1998). Accordingly, the current intensity and style of venting at the ODP Mound may not be representative of more vigorous hydrothermal activity responsible for the formation of Middle Valley ore deposits in the past.

Acknowledgments

The outcome of this study was highly dependant upon the skills, professionalism and able assistance of the Captain and crew of the *R/V Atlantis* and *DSV Alvin* team. We thank them for a highly successful and enjoyable cruise. Peter Saccocia, Tom McCollom, Karen Hurley, Hallie Marbet, and Dane Percy provided invaluable laboratory assistance aboard ship. We thank Meg Tivey, Tim Eglinton, and Tina Voelker for comments on an earlier draft of the manuscript. Rob Zierenberg was an invaluable source of insight into the nature and history of venting at the ODP Mound field. This work was funded by NSF OCE-9906752.

Associate editor: Jeffrey C. Alt

References

Alt, J.C., 1995. Subseafloor processes in mid-ocean ridge hydrothermal systems. In: Humphris, S.E., Zierenberg, R.A., Mullineaux, L.S., Thomson, R.E. (Eds.), *Seafloor Hydrothermal Systems: Physical, Chemical, Biological, and Geological Interactions*. Geophysical Monograph, vol. 91, pp. 85–114.

Ames, D.E., Franklin, J.M., Hannington, M.H., 1993. Mineralogy and geochemistry of active and inactive chimneys and massive sulfide, Middle Valley, northern Juan de Fuca Ridge: An evolving hydrothermal system. *Can. Mineral.* **31**, 997–1024.

Arnórsson, S., Gunnlaugsson, E., 1985. New gas geothermometers for geothermal exploration—Calibration and application. *Geochim. Cosmochim. Acta* **49**, 1307–1325.

Barnes, H.L., 1981. Measuring thermodynamically interpretable solubilities at high temperatures and pressures. In: Rickard, D.T., Wickman, F.E. (Eds.), *Chemistry and Geochemistry of Solutions at High Temperatures and Pressures*. Nobel Symp. Phys. Chem. Earth, , vol. 13/14, pp. 321–338.

Berner, U., Faber, E., Scheeder, G., Panten, D., 1995. Primary cracking of algal and landplant kerogens: kinetic models of isotope variations in methane, ethane and propane. *Chem. Geol.* **126**, 233–245.

Bischoff, J.L., Dickson, F.W., 1975. Seawater–basalt interaction at 200 °C and 500 bars: Implications for the origin of sea-floor heavy-metal deposits and the regulation of seawater chemistry. *Earth Planet. Sci. Lett.* **25**, 385–397.

Bischoff, J.L., Pitzer, K.S., 1989. Liquid–vapor relations for the system NaCl–H_2O: Summary of the P–T–x surface from 300 to 500 °C. *Am. J. Sci.* **289**, 217–248.

Bischoff, J.L., Rosenbauer, R.J., 1985. An empirical equation of state for hydrothermal seawater (3.2 percent NaCl). *Am. J. Sci.* **285**, 725–763.

Blochl, E., Rachel, R., Burggraf, S., Hafenbradl, D., Jannasch, H.W., Stetter, K.O., 1997. Pyrolobus fumarii, gen. and sp. nov., represents a novel group of archaea extending the upper temperature limit of life to 113 °C. *Extremophiles* **1**, 14–21.

Braun, R.L., Rothman, A.J., 1975. Oil-shale pyrolysis: Kinetics and mechanism of oil production. *Fuel* **54**, 129–131.

Burnham, A.K., Schmidt, B.J., Braun, R.L., 1995. A test of the parallel reaction model using kinetic measurements on hydrous pyrolysis residues. *Org. Geochem.* **23**, 931–939.

Butterfield, D.A., McDuff, R.E., Franklin, J., Wheat, C.G., 1994a. Geochemistry of hydrothermal vent fluids from Middle Valley, Juan de Fuca Ridge. In: Mottl, M.J., Davis, E.E., Fisher, A.T., Slack, J.F. (Eds.), *Proc. ODP, Sci. Results*, vol. 139, pp. 395–410.

Butterfield, D.A., McDuff, R.E., Mottl, M.J., Lilley, M.D., Lupton, J.E., Massoth, G.J., 1994b. Gradients in the composition of hydrothermal fluids from the Endeavour segment vent field: Phase separation and brine loss. *J. Geophys. Res.* **99**, 9561–9583.

Coleman, M.L., Risatti, J.B., Schoell, M., 1981. Fractionation of carbon and hydrogen isotopes by methane-oxidizing bacteria. *Geochim. Cosmochim. Acta* **45**, 1033–1037.

Cruse, A.M., 2002. Geochemistry of Hydrothermal Vent Fluids from the Northern Juan de Fuca Ridge. Ph.D. Thesis, Massachusetts Institute of Technology—Woods Hole Oceanographic Institution. 291 p.

Cruse, A.M., Seewald, J.S., 2001. Metal mobility in sediment-covered ridge-crest hydrothermal systems: Experimental and theoretical constraints. *Geochim. Cosmochim. Acta* **65**, 3233–3247.

Davis, E.E., Fisher, A.T., 1994. On the nature and consequences of hydrothermal circulation in the Middle Valley sedimented rift: Inferences from geophysical and geochemical observations, Leg 139. In: Mottl, M.J., Davis, E.E., Fisher, A.T., Slack, J.F. (Eds.), *Proc. ODP, Sci. Results*, vol. 139, pp. 695–717.

Davis, E.E. et al., 1992. *Proc. Ocean Drilling Program*, Init. Reports, vol. 139. Ocean Drilling Program.

Davis, E.E., Villinger, H., 1992. Tectonic and thermal structure of the Middle Valley sedimented rift, northern Juan de Fuca Ridge. In: Davis, E.E., Mottl, M.J., Fisher, A.T., et al. (Eds.), *Proc. ODP, Init. Reports*, vol. 139, pp. 9–41.

Davis, E.E., Wang, K., 1994. Present and past temperatures of sediments at Site 857, Middle Valley, northern Juan de Fuca Ridge. In: Mottl, M.J., Davis, E.E., Fisher, A.T., Slack, J.F. (Eds.), *Proc. ODP, Sci. Results*, vol. 139, pp. 565–570.

Des Marais, D.J., Donchin, J.H., Nehring, N.L., Truesdell, A.H., 1981. Molecular carbon isotopic evidence for the origin of geothermal hydrocarbons. *Nature* **292**, 826–828.

Des Marais, D.J., Stallard, M.L., Nehring, N.L., Truesdell, A.H., 1988. Carbon isotope geochemistry of hydrocarbons in the Cerro Prieto geothermal field, Baja California Norte, Mexico. *Chem. Geol.* **71**, 159–167.

Disnar, J.R., Sureau, J.F., 1990. Organic matter in ore genesis: Progress and perspectives. *Org. Geochem.* **16**, 577–599.

Edmond, J.M., Massoth, G., Lilley, M.D., 1992. Submersible-deployed samplers for axial vent waters. *RIDGE Events* **3**, 23–24.

Gieskes, J.M., Simoneit, B.R.T., Shanks III, W.C., Goodfellow, W.D., James, R.H., Baker, P.A., Ishibashi, J., 2002. Geochemistry of fluid phases and sediments: relevance to hydrothermal circulation in Middle Valley, ODP Legs 139 and 169. *Appl. Geochem.* **17**, 1381–1399.

Giggenbach, W.F., 1982. Carbon-13 exchange between CO_2 and CH_4 under geothermal conditions. *Geochim. Cosmochim. Acta* **46**, 159–165.

Golden, C.E., Webb, S.C., Sohn, R.A., 2003. Hydrothermal microearthquake swarms beneath active vents at Middle Valley, northern Juan de Fuca Ridge. *J. Geophys. Res.* **108**, 2027. doi:10.1029/2001JB000226.

Goodfellow, W.D., Blaise, B., 1988. Sulfide formation and hydrothermal alteration of hemipelagic sediment in Middle Valley, northern Juan de Fuca Ridge. *Can. Mineral.* **26**, 675–696.

Goodfellow, W.D., Peter, J.M., 1994. Geochemistry of hydrothermally altered sediment, Middle Valley, northern Juan de Fuca Ridge. In: Mottl, M.J., Davis, E.E., Fisher, A.T., Slack, J.F. (Eds.), *Proc. ODP, Sci. Results*, vol. 139, pp. 207–289.

Helgeson, H.C., 1991. Organic/inorganic reactions in metamorphic processes. *Can. Mineral.* **29**, 707–739.

Helgeson, H.C., Knox, A.M., Owens, C.E., Shock, E.L., 1993. Petroleum, oil field waters, and authigenic mineral assemblages: Are they in metastable equilibrium in hydrocarbon reservoirs? *Geochim. Cosmochim. Acta* **57**, 3295–3339.

Hessler, R.R., Kaharl, V.A., 1995. The deep-sea hydrothermal vent community: An overview. In: Humphris, S.E., Zierenberg, R.A., Mullineaux, L.S., Thomson, R.E. (Eds.), *Seafloor Hydrothermal Systems: Physical, Chemical, Biological, and Geological Interactions*. Geophysical Monograph, vol. 91, pp. 72–84.

Horita, J., 2001. Carbon isotope exchange in the system CO_2–CH_4 at elevated temperatures. *Geochim. Cosmochim. Acta* **65**, 1907–1919.

Hunt, J.M., 1985. Generation and migration of light hydrocarbons. *Science* **226**, 1265–1270.

Hunt, J.M., 1996. *Petroleum Geochemistry and Geochemistry*. W.H. Freeman.

Hunt, J.M., Whelan, J.K., Huc, A.-Y., 1980. Genesis of petroleum hydrocarbons in marine sediments. *Science* **209**, 403–404.

James, A.T., 1983. Correlation of natural gas by use of a carbon isotopic distribution between hydrocarbon components. *Am. Assoc. Petrol. Geol. Bull.* **67** (7), 1176–1191.

Janecky, D.R., Seyfried, W.E. Jr., Berndt, M.E., 1986. Fe–O–S redox reactions and kinetics in hydrothermal systems. In: *5th International Symposium on Water–Rock Interaction Extended Abstract*, pp. 282–285.

Johnson, J.W., Oelkers, E.H., Helgeson, H.C., 1992. SUPCRT92: A software package for calculating the standard molal thermodynamic properties of minerals, gases, aqueous species, and reactions from 1 to 5000 bar and 0 to 1000 °C. *Comput. Geosci.* **18**, 899–947.

Kashefi, K., Lovley, D.R., 2003. Extending the upper temperature limit for life. *Science* **301**, 934.

Kelley, D.S., Früh-Green, G.L., 1999. Abiogenic methane in deep-seated mid-ocean ridge environments: Insights from stable isotope analysis. *J. Geophys. Res.* **104**, 10439–14460.

Kiyosu, Y., Krouse, H.R., 1989. Carbon isotope effect during abiogenic oxidation of methane. *Earth Planet. Sci. Lett.* **95**, 302–306.

Koroleff, F., 1976. Determination of nutrients. In: Grasshoff, K. (Ed.), *Methods of Seawater Analysis*. Verlag-Chemie, pp. 125–157.

Krouse, H.R., Viau, C.A., Eliuk, L.S., et al., 1988. Chemical and isotopic evidence of thermochemical sulphate reduction by light hydrocarbon gases in deep carbonate reservoirs. *Nature* **333**, 415–419.

Lilley, M.D., Butterfield, D.A., Olson, E.J., et al., 1993. Anomalous CH_4 and NH_4^+ concentrations at an unsedimented mid-ocean-ridge hydrothermal system. *Nature* **364**, 45–47.

Lister, C.R.B., 1974. On the penetration of water into hot rock. *Geophys. J.* **39**, 465–509.

Lister, C.R.B., 1983. The basic physics of water penetration into hot rock. In: Rona, P.A., Boström, K., Smith, K.L., Jr.Jr. (Eds.), *Hydrothermal Processes at Seafloor Spreading Centers*. Plenum Press, pp. 141–168.

Lorant, F., Prinzhofer, A., Behar, F., Huc, A.-Y., 1998. Carbon isotopic and molecular constraints on the formation and the expulsion of thermogenic hydrocarbon gases. *Chem. Geol.* **147**, 249–264.

Martens, C.S., 1990. Generation of short-chain organic acid anions in hydrothermally altered sediments of the Guaymas Basin, Gulf of California. *Appl. Geochem.* **5**, 71–76.

McCollom, T.M., Seewald, J.S., Simoneit, B.R.T., 2001. Reactivity of monocyclic aromatic compounds under hydrothermal onditions. *Geochim. Cosmochim. Acta* **65**, 455–468.

Mottl, M.J., Holland, H.D., 1978. Chemical exchange during hydrothermal alteration of basalt by seawater—I. Experimental results for major and minor components of seawater. *Geochim. Cosmochim. Acta* **42**, 1103–1115.

Peter, J.M., Goodfellow, W.D., Leybourne, M.I., 1994. Fluid inclusion petrography and microthermometry of the Middle Valley hydrothermal system, northern Juan de Fuca Ridge. In: Mottl, M.J., Davis, E.E., Fisher, A.T., Slack, J.F. (Eds.), *Proc. ODP, Sci. Results*, vol. 139, pp. 411–422.

Pledger, R.J., Baross, J.A., 1991. Preliminary description and nutritional characterization of a heterotrophic archaeobacterium growing at temperatures of up to 110 °C isolated from a submarine hydrothermal vent environment. *J. Gen. Microbiol.* **137**, 203–211.

Rabinowicz, M., Boulègue, J., Genthon, P., 1998. Two- and three-dimensional modeling of hydrothermal convection in the sedimented Middle Valley segment, Juan de Fuca Ridge. *J. Geophys. Res.* **103**, 24045–24065.

Rice, D.D., Claypool, G.E., 1981. Generation, accumulation, and resource potential of biogenic gas. *AAPG Bull.* **65**, 5–25.

Rooney, M.A., Claypool, G.E., Chung, H.M., 1995. Modeling thermogenic gas generation using carbon isotope ratios of natural gas hydrocarbons. *Chem. Geol.* **126**, 219–232.

Sansone, F.J., Mottl, M.J., Olson, E.J., Wheat, C.G., Lilley, M.D., 1998. CO_2-depleted fluids from mid-ocean ridge-flank hydrothermal springs. *Geochim. Cosmochim. Acta* **62**, 2247–2252.

Schoell, M., 1980. The hydrogen and carbon isotopic composition of methane from natural gases of various origins. *Geochim. Cosmochim. Acta* **44**, 649–661.

Schoell, M., 1988. Multiple origins of methane in the Earth. *Chem. Geol.* **71**, 1–10.

Schofield, K., 1973. Evaluated chemical kinetic rate constants from various gas phase reactions. *J. Phys. Chem. Ref. Data* **2**, 25–84.

Seewald, J.S., 1994. Evidence for metastable equilibrium between hydrocarbons under hydrothermal conditions. *Nature* **370**, 285–287.

Seewald, J.S., 1997. Mineral redox buffers and the stability of organic compounds under hydrothermal conditions. In: Voight, J.A., Wood, T.E., Bunker, B.E., Casey, W.H., Crossey, L.J. (Eds.), *Aqueous Chemistry and Geochemistry of Oxides, Oxyhydroxides, and Related Materials, Materials Research Society Symposium Proceedings*, vol. 432, pp. 317–331.

Seewald, J.S., 2001a. Aqueous geochemistry of low molecular weight hydrocarbons at elevated temperatures and pressures: Constraints from mineral buffered laboratory experiments. *Geochim. Cosmochim. Acta* **65**, 1641–1664.

Seewald, J.S., 2001b. Model for the origin of carboxylic acids in basinal brines. *Geochim. Cosmochim. Acta* **65**, 3779–3789.

Seewald, J.S., Doherty, K.W., Hammar, T.R., et al., 2002. A new gas-tight isobaric sampler for hydrothermal fluids. *Deep-Sea Res. I* **49**, 189–196.

Seewald, J.S., Cruse, A.M., Saccocia, P., 2003. Aqueous volatiles in hydrothermal fluids from the Main Endeavour Field, northern Juan de Fuca Ridge: Temporal variability following earthquake activity. *Earth Planet. Sci. Lett.* **216**, 575–590.

Seewald, J.S., Seyfried Jr., W.E., 1991. Experimental determination of portlandite solubility in H_2O and acetate solutions at 100–350 °C and 500 bars; constraints on calcium hydroxide and calcium acetate complex stability. *Geochim. Cosmochim. Acta* **55**, 659–669.

Seewald, J.S., Seyfried Jr., W.E., Shanks III, W.C., 1994. Variations in the chemical and stable isotope composition of carbon and sulfur species during organic-rich alteration: An experimental and theoretical study at Guaymas Basin, Gulf of California. *Geochim. Cosmochim. Acta* **58**, 5065–5082.

Seyfried Jr., W.E., Bischoff, J.L., 1981. Experimental seawater–basalt interaction at 300 °C, 500 bars: Chemical exchange, secondary mineral formation and implications for the transport of heavy metals. *Geochim. Cosmochim. Acta* **45**, 135–149.

Seyfried Jr., W.E., Berndt, M.E., Seewald, J.S., 1988. Hydrothermal alteration processes at mid-ocean ridges: Constraints from diabase alteration experiments, hot-spring fluids and composition of the oceanic crust. *Can. Mineral.* **26**, 787–804.

Seyfried, W.E. Jr., Ding, K., 1995. Phase equilibria in subseafloor hydrothermal systems; a review of the role of redox, temperature, pH and dissolved Cl on the chemistry of hot spring fluids at mid-ocean ridges.in: Humphris, S.E., Zierenberg, R.A., Mullineaux, L.S., Thomson, R.E. (Eds.), *Seafloor Hydrothermal Systems: Physical, Chemical, Biological, and Geological Interactions*. Geophysical Monograph, vol. 91, pp. 248–272.

Seyfried Jr., W.E., Seewald, J.S., Berndt, M.E., Ding, K., Foustoukos, D., 2003. Chemistry of hydrothermal vent fluids from the Main Endeavour field, northern Juan de Fuca Ridge: Geochemical controls in the aftermath of June 1999 seismic events. *J. Geophys. Res.* **108**, 2429.

Shanks, W.C. III, 2001. Stable isotope systematics in seafloor hydrothermal systems: Vent fluids, hydrothermal deposits, hydrothermal alteration, and microbial processes. In: Valley, J.W., Cole, D.R. (Eds.), *Stable Isotope Geochemistry*, pp. 469–525.

Sherwood Lollar, B., Frape, S.K., Weise, S.M., Fritz, P., Macko, S.A., Welhan, J.A., 1993. Abiogenic methanogenesis in crystalline rocks. *Geochim. Cosmochim. Acta* **57**, 5087–5097.

Sherwood Lollar, B., Westgate, T.D., Ward, J.A., Slater, G.F., Lacrampe-Couloume, G., 2002. Abiogenic formation of alkanes in the Earth's crust as a minor source for global hydrocarbon reservoirs. *Nature* **416**, 522–524.

Shipboard Scientific Party, 1992. Site 858. In: Davis, E.E., Mottl, M.J., Fisher, A.T., et al. (Eds.), *Proc. ODP, Init. Reports*, vol. 139, pp. 431–569.

Shipboard Scientific Party, 1998a. Middle Valley: Bent Hill Area (Site 1035). In: Fouquet, Y., Zierenberg, R.A., Miller, D.J., et al. (Eds.), *Proc. ODP, Init. Reports*, vol. 169, pp. 35–152.

Shipboard Scientific Party, 1998b. Middle Valley: Dead Dog Area (Site 1036). In: Fouquet, Y., Zierenberg, R.A., Miller, D.J., et al. (Eds.), *Proc. ODP, Init. Reports*, vol. 169, pp. 153–203.

Shock, E., 1992. Chemical environments of submarine hydrothermal systems. *Origins Life Evol. Biosphere* **22**, 135–146.

Shock, E.L., 1988. Organic acid metastability in sedimentary basins. *Geology* **16**, 886–890.

Shock, E.L., 1989. Corrections to "Organic acid metastability in sedimentary basins". *Geology* **17**, 572–573.

Simoneit, B.R.T., 1994. Lipid/bitumen maturation by hydrothermal activity in sediments of Middle Valley, Leg 139. In: Mottl, M.J., Davis, E.E., Fisher, A.T., Slack, J.F. (Eds.), *Proc. ODP, Sci. Results*, pp. 447–464. Ocean Drilling Program.

Simoneit, B.R.T., Goodfellow, W.D., Franklin, J.M., 1992. Hydrothermal petroleum at the seafloor and organic matter alteration in sediments of Middle Valley, Northern Juan de Fuca Ridge. *Appl. Geochem.* **7**, 257–264.

Sleep, N.H., Morton, J.L., 1983. Heat loss and clogging beneath black-smoker vents. *Eos* **64**, 724.

Stakes, D.S., Schiffman, P., 1999. Hydrothermal alteration within the basement of the sedimented ridge environment of Middle Valley, northern Juan de Fuca Ridge. *GSA Bull.* **111**, 1294–1314.

Stein, J.S., Fisher, A.T., 2001. Multiple scales of hydrothermal circulation in Middle Valley, northern Juan de Fuca Ridge: Physical constraints and geological models. *J. Geophys. Res.* **106**, 8563–8580.

Stein, J.S., Fisher, A.T., Langseth, M., Jin, W., Iturrino, G., Davis, E., 1998. Fine-scale heat flow, shallow heat sources, and decoupled circulation systems at two hydrothermal sites, Middle Valley, northern Juan de Fuca Ridge. *Geology* **26**, 1115–1118.

Stetter, K.O., Fiala, G., Huber, G., Segerer, A., 1990. Hyperthermophilic microorganisms. *FEMS Microbiol. Rev.* **75**, 117–124.

Taylor, B.E., 1992. Degassing of CO2 from Kilauea: Carbon isotopic evidence and implications for magmatic contributions to sediment-hosted submarine hydrothermal systems. *Rept. Geol. Surv. Japan* **279**, 205–206.

Tissot, B., Welte, D.H., 1984. *Petroleum Formation and Occurrence*. Verlag.

Von Damm, K.L., Edmond, J.M., Grant, B., Measures, C.I., Walden, B., Weiss, R.F., 1985. Chemistry of submarine hydrothermal solutions at 21 °N, East Pacific Rise. *Geochim. Cosmochim. Acta* **49**, 2197–2220.

Von Damm, K.L., Oosting, S.E., Kozlowski, R., Buttermore, L.G., Colodner, D.C., Edmonds, H.N., Edmond, J.M., Grebmeier, J.M., 1995. Evolution of East Pacific Rise hydrothermal vent fluids following a volcanic eruption. *Nature* **375**, 47–50.

Von Damm, K.L., Parker, C.M., Zierenberg, R.A., Lilley, M.D., Olson, E.J., Clague, E.J., McClain, J.S., 2005. The Escanaba Trough, Gorda Rigde hydrothermal system: Temporal stability and seafloor complexity. *Geochim. Cosmochim. Acta* **69**, 4971–4984.

Waples, D.W., 1984. Thermal models for oil generation. In: Brooks, J., Welte, D. (Eds.), *Advances in Petroleum Geochemistry*, vol. 1, pp. 7–67.

Welhan, J.A., 1988. Origins of methane in hydrothermal systems. *Chem. Geol.* **71**, 183–198.

Whelan, J.K., Simoneit, B.R.T., Tarafa, M.E., 1988. C_1–C_8 hydrocarbons in sediments from Guaymas Basin, Gulf of California–Comparison to Peru Margin, Japan Trench and California Borderlands. *Org. Geochem.* **12**, 171–194.

Whiticar, M.J., 1999. Carbon and hydrogen isotope systematics of bacterial formation and oxidation of methane. *Chem. Geol.* **161**, 291–314.

Whiticar, M.J., Faber, E., Whelan, J.K., Simoneit, B.R.T., 1994. Thermogenic and bacterial hydrocarbon gases (free and sorbed) in Middle Valley, Juan de Fuca Ridge, Leg 139. In: Mottl, M.J., Davis, E.E., Fisher, A.T., Slack, J.F. (Eds.), *Proc. ODP, Sci. Results*, vol. 139, pp. 467–477.

Zhang, Q.-L., Wen-Jun, L., 1990. A calibrated measurement of the atomic weight of carbon. *Chinese Sci. Bull.* **35**, 290–296.

Zierenberg, R.A. et al., 1998. The deep structure of a sea-floor hydrothermal deposit. *Nature* **392**, 485–488.

Zierenberg, R.A., Miller, D.J., 2000. Overview of Ocean Drilling Program Leg 169: Sedimented Ridges II. In: Zierenberg, R.A., Fouquet, Y., Miller, D.J., Normark, W.R. (Eds.), *Proc. ODP, Sci. Results*, vol. 169 [Online]. Available from <http://www-odp.tamu.edu/publications/169_SR/VOLUME/CHAPTERS/SR169_10.PDF>.